

A Novel Ferrocenyl Naphthoquinone Fused Crown Ether as a Multisensor for Water Determination in Acetonitrile and Selective Cation Binding

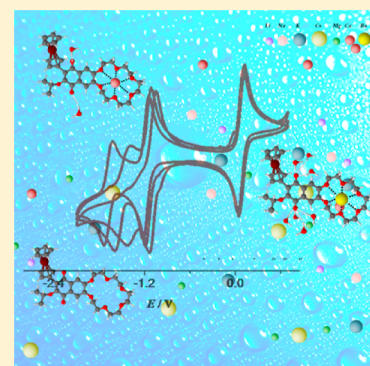
Metin Dagdevren,[†] Ismail Yilmaz,^{*,†} Baris Yucel,[†] and Mustafa Emirik[‡]

[†]Department of Chemistry, Istanbul Technical University, 34469, Maslak, Istanbul, Turkey

[‡]Department of Chemistry, Recep Tayyip Erdoğan University, 53100, Rize, Turkey

Supporting Information

ABSTRACT: A multisensor which is based on a novel multifunctional triad molecule, ferrocenyl naphthoquinone fused crown ether (**Fc-cnq**) bearing ferrocene, quinone, and crown ether functional groups together, was synthesized and characterized in this study. Sensing performance of a trace amount of water and the selective cation binding capabilities of this multisensor were carried out by the electrochemical, spectroelectrochemical, and spectrophotometric titration techniques in acetonitrile (CH₃CN). It was shown that the potential separation ($E^{(\text{Fc})}_{1/2} - E^{(2)}_{1/2}$) between the second reduction of naphthoquinone and the oxidation processes of ferrocene in the triad molecule **Fc-cnq** was proportional to the amount of water due to the hydrogen-bonding interactions between water and the doubly reduced species (**Fc-cnq**²⁻). This property enabled **Fc-cnq** to detect the trace amount of water in CH₃CN. The half-wave potential ($E^{(\text{Fc})}_{1/2}$) of the ferrocene in **Fc-cnq** was used as an internal reference potential, and it defined the accuracy of the detection. In addition, by using the UV-vis spectrophotometric titration technique in CH₃CN, it was also shown that the **Fc-cnq** multisensor could bind Ba²⁺ and Ca²⁺ cations selectively. We proposed that the intramolecular charge-transfer (CT) transition which occurred between the donor ferrocene and the acceptor naphthoquinone was the principle mechanism for the selective binding property of this multisensor. Quantum chemical calculations were also performed to investigate optical and electronic properties of the **Fc-cnq** molecule.



INTRODUCTION

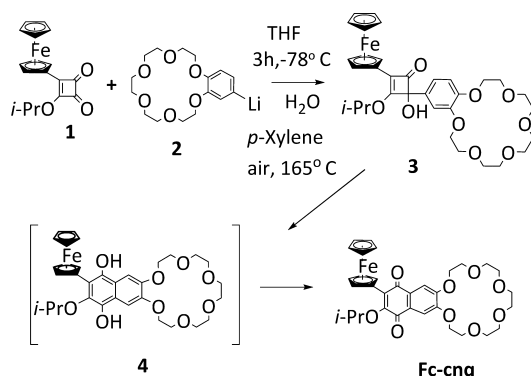
Multifunctional molecular materials that exhibit more than one property within the same molecule are an increasingly important challenge in many high-tech and medical applications.^{1–7} Therefore, many works have been recently focused on the design and synthesis of various multifunctional materials to especially implement for multisensor purposes.^{8,9} Nowadays, sensor research is shifting toward the development of multiparametric sensing, particularly of core analytes such as O₂, pH, CO₂, temperature, moisture, and ions, as well as of more simple, robust, versatile, and cost-efficient systems tailored to specific applications.^{8–10} For a long time, ferrocenes, quinones, and crown ethers, separately or their dyad, have been extensively facilitated in several applications such as environmental, clinical, chemical, biological, and particularly material science as well as sensor applications because of their well-documented unique properties such as thermal and chemical stability, electron/proton transfer processes with tunable redox potential, remarkable metal/molecular binding properties, and electron donor/acceptor nature.^{11–34} They have been actively studied throughout the development of the instrumentation and theory behind modern analytic techniques.^{35,36} According to our literature survey, ferrocene–quinone–crown ether molecular triads have not been investigated yet, although ferrocene–quinone,^{37–39} ferrocene–crown ether,^{25,26,34,40–44}

or quinone–crown ether^{45–48} molecular dyads have been reported to fulfill varying applications. Therefore, in this work, we have designed a ferrocene–quinone–crown ether molecular triad (**Fc-cnq**) as a multisensor for both determination of trace water in organic solvents and selective sensing of Ca²⁺ and Ba²⁺ in alkali and alkaline earth metal cations. The triad **Fc-cnq** was constructed using a regiospecific method involving thermal rearrangement of the reactive ferrocenyl-substituted 4-hydroxy-4-(benzoyl-18-crown-6)cyclobutenone (**3**) to intermediate hydroquinone (**4**) and its following *in situ* oxidation under air atmosphere (Scheme 1).

Water is essential for daily life, and often used in the preparation of many materials. However, the presence of even a very low level of water in the industrial and medical products or in the organic solvents is one of the most common contaminants. Therefore, determination of water is of great industrial and environmental importance, and one of the most common routine procedures in many research and industrial processes.^{49–53} So far, many methods such as spectroscopic, amperometric, and gravimetric methods have been developed for water determination, of which the Karl Fischer method has

Received: July 9, 2015

Revised: August 24, 2015

Scheme 1. Synthesis of Ferrocenyl Naphthoquinone Fused Crown Ether (Benzo-18-crown-6) Fc-cnq

been used mostly.^{54–57} Recently, it was found that the potential separations between the first and second reduction processes of quinones were especially sensitive to water in the low molar levels, which could nicely be applied to determine the moisture content of nonaqueous solvents based on hydrogen-bonding interactions between water and two-electron reduced forms of vitamin K₁.^{51,52} In the same year, a similar study was carried out using some quinones such as tetrachloro-*p*-benzoquinone, benzoquinone, and tetramethyl-*p*-benzoquinone.⁵⁰ In our study, first, ferrocenyl naphthoquinone **Fc-cnq** was used to determine a trace amount of water in the solvent of acetonitrile (CH₃CN) by using the voltammetric technique, where CH₃CN was especially chosen as a model organic aprotic solvent for nonaqueous electrochemical measurements. The voltammetric determination of a trace amount water in CH₃CN has been performed by using the hydrogen-bonding interactions between water and the reduced species (Fc-cnq²⁻) and the electrochemical collaboration of quinone and ferrocene in the molecule **Fc-cnq**. The potential separations ($E_{1/2}$, half-wave potential) between the second reduction of naphthoquinone and the oxidation processes of ferrocene, estimated by using **Fc-cnq**, were for the first time applied for the voltammetric determination of a trace amount of water in CH₃CN, where the oxidation potential of ferrocene remained stable as water was added into the solution. Hence, it is a significant advantage that the $E^{(Fc)}_{1/2}$ of the ferrocene in the molecule can be used as an internal reference potential for accurate water determination in the solvent.

The selective binding ability of crown ethers is widely accepted in molecular recognition.^{25–34,40–44} They are also frequently used as ion sensors in selective electrode in analytical chemistry.^{58–60} Calcium is an essential nutrient, and is the most abundant element in the human body. On the other hand, Ba²⁺ ion especially plays an important role in biological systems. For example, elevated levels of Ba²⁺ in humans can cause acute gastroenteritis, loss of deep reflexes, muscular paralysis, respiratory failure, or even death.³⁶ Therefore, many efforts have been devoted for sensing of Ca²⁺ and Ba²⁺.³⁶ In this study, second, the designed molecule **Fc-cnq** was utilized as a selective metal sensor toward Ba²⁺ and Ca²⁺ cations in CH₃CN solution, which was based on the ion–dipole interactions between macrocyclic ring and cations. This interaction caused the intramolecular charge-transfer (CT) transition between the ferrocenyl donor and naphthoquinonyl acceptor center [e_{π} (HOMO–Fc) \rightarrow e_{π^*} (LUMO–cnq)] to shift toward lower energy.

Several recent studies show that the course of electroreduction for quinones is remarkably complex in the acidic medium.^{18,20,35,36,61–68} As a third application, we have also presented an electrochemical approach to understand electron and proton-coupled electron transfer of the ferrocenyl naphthoquinones in nonaqueous solutions in the presence of weak and strong organic acids such as acetic acid (AcOH) and trifluoroacetic acid (TFA), thereby possibly evaluating the molecule **Fc-cnq** as a pH sensor.

EXPERIMENTAL SECTION

General Considerations. All reagents were used as purchased from commercial suppliers without further purification unless otherwise indicated. Diethyl ether and THF were freshly distilled from sodium/benzophenone ketyl. Electrochemical grade acetonitrile (CH₃CN) was purchased from commercial suppliers, but a method was applied to prepare ultradry CH₃CN as followed. The solvent of CH₃CN was first distilled over P₂O₅ under a vacuum and then transferred in a homemade glass apparatus containing the activated 3 Å molecular sieve under a vacuum desiccator at least for 3 days. The molecular sieve was activated at 573 K in an oven and then transferred to the homemade glass apparatus allowed to cool under an argon atmosphere. The water content of the ultradry CH₃CN tested by Karl Fischer (KF) titration was found below 20 ppm in our experimental conditions. Tetra-*n*-butylammonium perchlorate used as supporting electrolyte (*n*-Bu₄NClO₄, Fluka Chemical Co.) was recrystallized from ethyl alcohol and dried in a vacuum oven at 40 °C for at least 1 week prior to use. Solvents for column chromatography, ethyl acetate, and hexane were distilled in a rotary evaporator. Chromatographic separations were performed with Merck Silica 60 (200–400 or 70–230 mesh). TLC was performed with Merck TLC Silicagel 60 F254 plates, and detection was carried out under UV light at 254 nm.

Measurements. NMR spectra were recorded with an Agilent VNMRs 500 (500 MHz for ¹H and 125 MHz for ¹³C NMR) instrument. Chemical shifts δ were given in ppm relative to residual peaks of deuterated solvents, and coupling constants, *J*, were given in Hertz. The following abbreviations are used to describe spin multiplicities in ¹H NMR spectra: s = singlet; d = doublet; t = triplet; q = quartet; dd = doublet of doublets; m = multiplets. IR spectra were recorded on a Perkin–Elmer FT-IR spectrometer. Low resolution mass spectra (API-ES, 70 eV, and APCI) were obtained on an Agilent 1100 LC-MS instrument equipped with a diode array UV–visible (UV–vis) range detector and Thermo LCQ Deca Ion Trap Mass Spectrometer (Thermo Finnigan). High resolution mass spectra (HRMS) were obtained on a Waters Synapt Q-TOF-MS spectrometer. Elemental analysis was carried out by the CHNS Elemental Analyzer instrument in TÜBITAK (MAM). UV–visible spectra were recorded on an Agilent model 8453 diode array spectrophotometer. Cyclic voltammograms (CVs) were carried out using CV measurements with a Princeton Applied Research model 2263 potentiostat controlled by an external PC. A three-electrode system [BAS model (Bioanalytical System Inc.) solid cell stand] was used for CV measurements in CH₃CN, and it consisted of platinum (1.6 mm diameter) and glassy carbon (3.0 mm diameter) disc electrodes as the working electrode, a platinum wire counter electrode, and a Ag/AgNO₃ (nonaqueous) reference electrode. The reference electrode was separated from the bulk solution by a fritted-glass bridge filled with the

solvent/supporting electrolyte mixture. The ferrocenium/ferrocene couple (Fc^+/Fc) was used as an internal standard, but all potentials in the paper are referenced to the Ag/Ag^+ (nonaqueous) reference electrode. Solutions containing **Fc-cnq** were deoxygenated by a stream of high purity argon for 35 min before running the experiment, and the solution was protected from air by a blanket of argon during the experiment. The sample and solvent were placed into the electrolysis cell under nitrogen. The platinum electrode was polished on alumina ($<10\ \mu\text{M}$) slurries on a BAS felt pad. This was followed by rinsing with Millipore water and then ethanol. UV-vis spectroelectrochemical experiments were performed with a home-built thin-layer cell that utilized a light transparent platinum gauze working electrode.⁶⁹ Potentials were applied and monitored with a Princeton Applied Research model 2263 potentiostat. Time-resolved UV-vis spectra were recorded on an Agilent model 8453 diode array spectrophotometer. Cation binding study was performed with the UV-vis spectrophotometric titration technique at $25 \pm 0.02\ ^\circ\text{C}$. Three mL and $1.0 \times 10^{-4}\ \text{M}$ of **Fc-cnq** in CH_3CN was taken into the cell for UV-vis titration with increasing concentrations of alkaline (Li^+ , Na^+ , K^+ , and Cs^+) and earth alkaline metal (Mg^{2+} , Ca^{2+} , and Ba^{2+}) perchlorates. It should be noted that metal perchlorates were prepared more concentrated to prevent observation of dilution effects. Conductivity measurements were carried out with a WTW pH/conc. 720 conductivity meter. A dip-type conductivity cell, made of platinum black, with a cell constant of $0.8\ \text{cm}^{-1}$ was used. In order to avoid dilution effects by adding a crown ether solution to a salt solution, the conductance was monitored at constant salt concentration, and dilute acetonitrile solutions of the metal perchlorates were used in the present study. The experimental procedures to obtain equivalent conductivity of mono- and univalent cation perchlorate solution containing **Fc-cnq** are as follows: 40 mL of alkali metal perchlorate solution ($1.0 \times 10^{-4}\ \text{M}$) was placed in the titration cell and thermostated to $25.00 \pm 0.02\ ^\circ\text{C}$, and the conductance of the solution was measured. Then, a step-by-step increase of **Fc-cnq** concentration was effected by a titration with a micropipette from the solution of **Fc-cnq**/salt mixture to the vessel. The solution was stirred magnetically. Addition of the ligand was continued until the desired ligand-to-cation mole ratio was achieved. In all electrochemical experiments, KF titrations were conducted with a Mettler-Toledo C20 coulometer to determine a trace amount of water in solvents studied, for which Combi Coulamat Fritless KF solution (Merck) was used in the experiment.

Synthesis of 19-Isopropoxy-20-ferrocenyl-2,3,6,9,11,12,14,15-decahydronaphtho[2,3-b]-[1,4,7,10,13,16]hexaoxacyclooctadecine-18,21-dione (Fc-cnq). To a solution of 4'-bromo-benzo-18-crown-6 (0.58 g, 1.48 mmol) in THF at $-78\ ^\circ\text{C}$ under nitrogen, *n*-BuLi (1.25 mL or 2.4 equiv of a 1.6 M hexane solution) was added via syringe in 15 min. The resulting mixture containing **2** was stirred at $-78\ ^\circ\text{C}$ for 1 h and then transferred via cannula to a solution of 3-ferrocenyl-4-isopropoxy-3-cyclobutene-1,2-dione (**1**) (0.53 g or 1.63 mmol) in THF at $-78\ ^\circ\text{C}$ under the nitrogen atmosphere. After stirring for 3 h at $-78\ ^\circ\text{C}$, the reaction mixture was quenched with H_2O at $-78\ ^\circ\text{C}$ and then allowed to warm to room temperature. The mixture diluted with ether (50 mL) and the organic layer was separated. The aqueous layer was extracted with ether ($2 \times 25\ \text{mL}$). The combined organic layers were dried over Mg_2SO_4 and filtered. The solution concentrated in a rotary evaporator and the

remaining crude material was dissolved in *p*-xylene. The resulting solution was heated at reflux open to the air in a preheated oil bath ($165\ ^\circ\text{C}$) for 3 h. After removal of the *p*-xylene in a rotary evaporator, the residue was dissolved in 25 mL of ether and 2 g of silica gel was added into the solution. The solution again was concentrated in a rotary evaporator and the green solid residue was subjected to the chromatography on silica gel using 1:3 hexane/ethyl acetate as eluent to yield **Fc-cnq** (0.50 g, 53%, green solid). ^1H NMR (500 MHz, CDCl_3): $\delta = 1.30$ (d, $J = 6.1\ \text{Hz}$, 6 H, $2 \times i\text{PrO} [\text{CH}_3]$), 3.72–3.81 (m, 12 H, $6 \times \text{CH}_2$), 4.0 (s, 4 H, $2 \times \text{CH}_2$), 4.22 (s, 5 H, Fc), 4.32–4.35 (m, 4 H, $2 \times \text{CH}_2$), 4.59 (s, 2 H, Fc), 4.81–4.86 (m, 1 H, *i*PrO $[\text{CH}]$), 5.26 (s, 2 H, Fc), 7.46 (s, 1 H, Ar), 7.49 (s, 1 H, Ar); ^{13}C NMR (125 MHz, CDCl_3): $\delta = 22.82$ ($2 \times \text{CH}_3$, *i*PrO), 69.04 ($6 \times \text{CH}_2$), 70.13 ($4 \times \text{CH}_2$), 70.41 ($5 \times \text{CH}$, Fc), 70.62 ($2 \times \text{CH}$, Fc), 70.84 ($2 \times \text{CH}$, Fc), 72.87 (C_{quat} , Fc), 76.31 (CH, *i*PrO), 108.38 (CH, Ar), 109.20 (CH, Ar), 125.92 (C_{quat}), 127.50 (C_{quat}), 130.87 (C_{quat}), 132.24 (C_{quat}), 153.50 (C_{quat}), 154.42 (C_{quat}), 180.54 (C_{quat} , $\text{C}=\text{O}$), 184.16 (C_{quat} , $\text{C}=\text{O}$); IR (ATR): $\tilde{\nu}$ (cm^{-1}) = 3081, 2929, 2877, 1658, 1583, 1502, 1461, 1311, 1253, 1179, 1121, 937, 909, 739; HRMS [TOF MS ES⁺]: m/z [M]⁺ Anal. Calcd for $\text{C}_{33}\text{H}_{38}\text{O}_9\text{NaFe}$: 657.1763 g/mol, found 657.1763 (0.0 ppm); E.A. Anal. Calcd for ($\text{C}_{33}\text{H}_{38}\text{O}_9\text{NaFe} \cdot \text{H}_2\text{O}$) C, 58.67, H, 5.97, found C, 58.65, H, 5.95.

Computational Details. All computations were done using the Gaussian 09⁷⁰ package. The geometry of the molecule under study was first optimized at the DFT^{71,72} (density functional theory) level with the exchange-correlation functional of Perdew and co-workers as modified by Adamo and Barone (mPWPW91)⁷³ and the 6-31+G(2d,2p) basis set without any symmetry constraint. Stationary points were confirmed to be local minima by performing analytic computations of vibrational frequencies with no imaginary frequency. On the basis of the optimized geometries, absorption spectra have been calculated by the time dependent DFT (TD-DFT)⁷⁴ formalism with the B97D⁷⁵ functional and the TZVP⁷⁶ basis set for 60 singlet–singlet excitations. Implicit solvent (acetonitrile) was included in both DFT and TD-DFT calculations by using the polarizable continuum model.⁷⁷

RESULTS AND DISCUSSION

Synthesis of Ferrocenyl Naphthoquinone Fused Crown Ether (Fc-cnq). The reaction route for the synthesis of ferrocenyl naphthoquinone fused crown ether (benzo-18-crown-6) **Fc-cnq** is presented in Scheme 1. Ferrocenyl naphthoquinone fused crown ether **Fc-cnq** was synthesized by the reaction of 3-ferrocenyl-4-isopropoxy-3-cyclobutene-1,2-dione^{37,38,78} (**1**) and lithio-benzo-18-crown-6 ether **2** according to the literature procedure.³⁷ Lithio-benzo-18-crown-6 ether (**2**) was prepared from 4'-bromo-benzo-18-crown-6⁷⁹ and *n*-butyllithium (*n*-BuLi) as a mixture in THF at low temperature ($-78\ ^\circ\text{C}$) under a nitrogen atmosphere in 1 h. The mixture was then transferred by means of a cannula into **1** in a different reaction vessel at low temperature ($-78\ ^\circ\text{C}$) under a nitrogen atmosphere. The synthesis of **Fc-cnq** was achieved without isolation and purification of ferrocenyl-substituted 4-hydroxy-4-(benzoyl-18-crown-6)cyclobutenone (**3**) which was dissolved in *p*-xylene as a crude product and refluxed open to air to promote oxidation of the intermediate hydroquinone **4**. The reaction was monitored by observing the change in color of the solution from deep purple to deep green, which was finalized when the color change persisted with disappearance of **3**.

Ferrocenyl naphthoquinone fused crown ether **Fc-cnq** was obtained in 53% yield after *p*-xylene was evaporated at a vacuum and column chromatography was carried out. By this way, the target molecule **Fc-cnq** was accomplished in a shorter time and consumed less chemicals such as solvents and silica gel. It was well-known that the isolation of the 4-hydroxycyclobutenone derivatives by the column chromatography was considerably tedious and they rapidly decomposed when they were kept even under the nitrogen atmosphere at room temperature. **Fc-cnq** could not be obtained when the NH_4Cl solution was used as a quencher according to the procedure given in the literature,³⁷ probably due to binding of NH_4^+ cation with crown ether macrocyclic. Hence, the reaction mixture was quenched with water instead of NH_4Cl solution in this reaction. In this work, we employed the method of the thermal rearrangements of the reactive 4-hydroxy-4-(benzoyl-18-crown-6)cyclobutenone (**5**) to achieve **Fc-cnq** after the oxidation of initially formed hydroquinone **4** (Scheme 1S). Ferrocenyl naphthoquinone fused crown ether **Fc-cnq** was elucidated by various techniques such as elemental analysis, FT-IR, ^1H and ^{13}C NMR, HRMS, and UV-vis, as shown in Figures 2S–5S and Figure 12.

Electrochemistry and Spectroelectrochemistry of Ferrocenyl Naphthoquinone Fused Crown Ether (Fc-cnq**).** Mechanistic study of electron transfer and hydrogen bonding processes of **Fc-cnq** was investigated by cyclic voltammetry (CV) in the solution of acetonitrile (CH_3CN) with and without water. The experiments were also carried out in the presence of weak (acetic acid, AcOH) and strong (trifluoroacetic acid, TFA) organic acids in the same solution to explore proton-coupled electron transfer processes. Tetra-*n*-butylammonium perchlorate ($n\text{-Bu}_4\text{NClO}_4$, 0.2 M) was used as a supporting electrolyte in the experiment. The CVs of **Fc-cnq** at varying scan rates (0.025–0.500 V s^{-1}) in CH_3CN are shown in Figure 1. It can be seen that **Fc-cnq** exhibits a chemically reversible one-electron reduction process to form semiquinone radical product, monoanion ($\text{Fc-scncq}^{\bullet-}$) at $E^{(1)}_{1/2} = -1.19$ V [ΔE_p (the anodic to cathodic peak-to-peak separation) = 0.0640 V, I_{pc}/I_{pa} (the anodic–cathodic peak ratio) = 0.96]. Following one-electron reduction is observed at a more

negative potential as a quasi-reversible process at $E^{(2)}_{1/2} = -1.72$ V; $\Delta E_p = 0.137$ V to form the doubly reduced product, dianion (Fc-cnq^{2-}) at a scan rate of 0.100 V s^{-1} (dark cyan line in Figure 1). **Fc-cnq** also displays a chemically reversible one-electron oxidation process corresponding to the ferrocenium/ferrocene (Fc^+/Fc) couple at $E^{(\text{Fc})}_{1/2} = 0.087$ V ($\Delta E_p = 0.0640$ V, $I_{pa}/I_{pc} = 0.98$). The reduction and oxidation processes were similar to typical CVs of benzoquinone, naphthoquinone, and ferrocene derivatives in aprotic organic solvents without water and acidic ingredients.^{20,37,50–52,61–63} The electron transfer mechanism for the electrochemical reaction of **Fc-cnq** in nonaqueous CH_3CN solution was depicted in Scheme 2 (in the direction of the blue

Scheme 2. Electrochemical Reduction and Oxidation Mechanism for **Fc-cnq in CH_3CN (the Pathways Indicated by Blue Double Arrows), after Addition of Water (the Pathways Indicated by Red Double Arrows), and Weak Organic Acid (AcOH) (the Pathways Indicated by Green Double Arrows) into the Solution of CH_3CN**

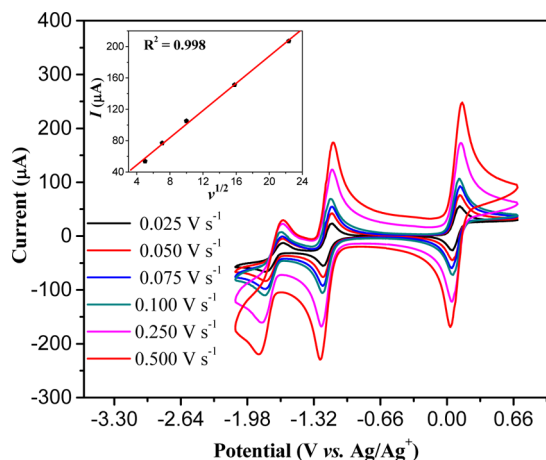
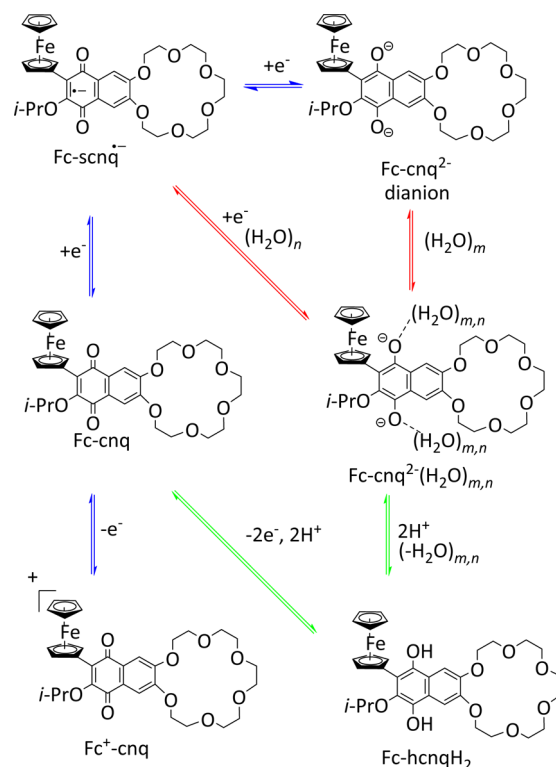


Figure 1. CVs of **Fc-cnq** in CH_3CN solution containing 0.2 M $n\text{-Bu}_4\text{NClO}_4$ at different scan rates (0.025–0.50 V s^{-1}). The concentration of **Fc-cnq** is 5.0×10^{-3} M. Inset: plot of $v^{1/2}$ vs. current. Working electrode: glassy carbon disk electrode (3.0 mm diameter).

double arrows). The anodic peak current observed for the second reduction process is smaller than that for the first reduction process, which can be clearly seen from Figure 1. The loss of the current is probably based on a complexation reaction between the doubly reduced product (Fc-cnq^{2-}) and the neutral state of the molecule **Fc-cnq** or an adsorption of the reduced species on the electrode surface, which was previously mentioned for several quinones in aprotic media.^{20,80} The difference between the half-wave potentials of the oxidation and the first reduction processes [$\Delta E_p = E^{(\text{Fc})}_{1/2}(\text{Fc}^+/\text{Fc}) - E^{(1)}_{1/2}(\text{Fc-scncq}^{\bullet-}/\text{Fc-cnq})$], related with the energy of the intramolecular charge-transfer transition between the ferrocenyl donor and naphthoquinonyl acceptor centers [e_π (HOMO-Fc) $\rightarrow e_\pi^*$ (LUMO-cnq)], was found to be 1.28 V. The difference between the half-wave potentials of the first and

second reduction processes [${}^2\Delta E_p = E^{(1)}_{1/2}(\text{Fc-cnq}/\text{Fc-scnq}^{\bullet-}) - E^{(2)}_{1/2}(\text{Fc-scnq}^{\bullet-}/\text{Fc-cnq}^{2-})$] for **Fc-cnq** was calculated as 0.530 V. The ${}^1\Delta E_p$ and ${}^2\Delta E_p$ values of **Fc-cnq** showed a good agreement with those of the ferrocenyl naphthoquinones bearing different substituents in the same experimental conditions.³⁷ For the ferrocene molecule, under our experimental conditions, $E_{1/2}$ of Fc^+/Fc was calculated as $E_{1/2} = 0.0690$ V ($\Delta E_p = 0.0850$ V) at a scan rate of 0.100 V s^{-1} , which can be used as a criterion for electrochemical reversibility.⁸¹ The redox processes of **Fc-cnq** were examined as a function of potential scan rate in order to ascertain the mode of mass transport. The cathodic and anodic currents for the oxidation and reduction couples in CH_3CN increased in direct proportion to the square root of scan rates between 0.025 and 0.500 V s^{-1} . Thus, this implied that the redox reactions in the solution were controlled by diffusion (inset in Figure 1).^{81–85}

Spectroelectrochemical properties of **Fc-cnq** were investigated by an *in situ* spectroelectrochemical technique combining chronoamperometry and UV–vis spectroscopy in a thin-layer cell.^{82–85} Experiment was performed in CH_3CN solution containing 0.2 M $n\text{-Bu}_4\text{NClO}_4$ electrolyte. The UV–vis spectral changes of the reduced and oxidized species for **Fc-cnq** were monitored while convenient potentials were applied in the thin-layer cell. The applied potential values (E_{app}) for the *in situ* spectroelectrochemical experiment were determined for each process by taking the CV of **Fc-cnq** in the same experimental condition. The E_{app} values for the first reduction and oxidation processes were found as -1.65 and 0.69 V poised just beyond the first cathodic and anodic waves. The UV–vis spectral changes during the formation of the reduced product of **Fc-cnq** were represented in Figure 2.

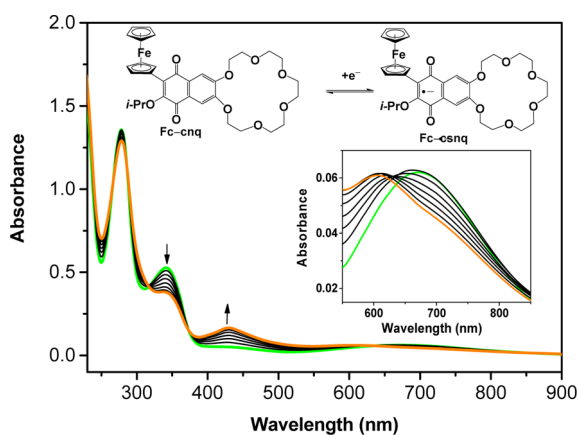


Figure 2. Time-resolved UV–vis spectral changes of **Fc-cnq** during the first reduction at $E_{\text{app}} = -1.65$ V in CH_3CN solution containing 0.2 M $n\text{-Bu}_4\text{NClO}_4$. Arrows mark the direction of absorbance change.

The spectrum of the reduced species, semiquinone radical anion ($\text{Fc-scnq}^{\bullet-}$), exhibited well-defined isosbestic points appearing at 317, 374, and 634 nm. This confirmed that the electrode reaction proceeded in a quantitative fashion and in the absence of any coupled chemistry.^{82–85} As seen from Figure 2, noticeable changes on band positions and in intensity for the spectrum of the reduced product (orange line) were observed when compared to the original spectrum of the neutral form (green line). This was as a result of addition of one electron into the LUMO level of the molecule. The bands at 277 and 341 nm were decreased in intensity, and new bands at 430 and

605 nm appeared. The characteristic intramolecular charge-transfer (CT) band observed at 666 nm was diminished by means of a newly formed electron-rich semiquinone center ($\text{Fc-scnq}^{\bullet-}$). The electrochemical reaction could be clearly monitored by the changing color of the solution from deep green to yellow in the thin-layer cell which confirmed the formation of the reduced product. Additionally, the original green color and the spectrum of **Fc-cnq** could be recovered upon reoxidation operation ($E_{\text{app}} = -0.66$ V) during the spectroelectrochemical measurements, indicating that the semiquinone radical anion ($\text{Fc-scnq}^{\bullet-}$) remained chemically stable throughout the experiment. The spectrum of the reduced product presented a characteristic view for a semiquinone radical anion ($\text{Fc-scnq}^{\bullet-}$) which was consistent with previously described ferrocene–benzoquinone systems.³⁷ The controlled potential coulometric study indicated that the number of electrons transferred for the forward and reverse electrochemical reactions of the complex was one for both the reduction and reoxidation processes based on the $\text{Fc-cnq}/\text{Fc-scnq}^{\bullet-}$ couple. After electrolysis ($E_{\text{app}} = -2.10$ V) was completed within 30 s to afford the doubly reduced forms (Fc-cnq^{2-}), the bands at 430 and 605 nm completely disappeared. The second reduction process could not be reversed upon the applied potential ($E_{\text{app}} = -0.66$ V) to recover the neutral state **Fc-cnq**, probably due to the complexation reaction between the dianion (Fc-cnq^{2-}) and neutral **Fc-cnq** forms or decomposition of more reduced species (Fc-cnq^{2-}) in the thin-layer cell. Figure 3 depicts the UV–vis spectral

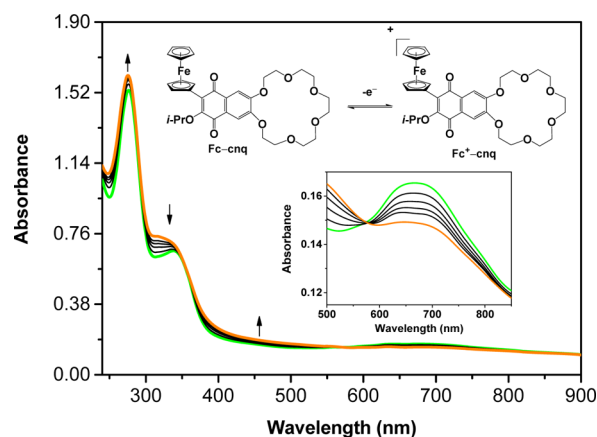


Figure 3. Time-resolved UV–vis spectral changes of **Fc-cnq** during the first oxidation at $E_{\text{app}} = 0.69$ V in CH_3CN solution containing 0.2 M $n\text{-Bu}_4\text{NClO}_4$. Arrows mark the direction of absorbance change.

changes during the oxidation process based on $\text{Fc}^+/\text{Fc-cnq}$ couples at $E_{\text{app}} = 0.690$ V. As expected, the intensity of the CT band (green line) almost disappeared by removing one electron from the HOMO level of the molecule during the oxidation process, thereby forming the mono cationic species ($\text{Fc}^+/\text{Fc-cnq}$). As observed for the first reduction process, all of the spectroscopic changes were fully reversed by a re-reduction process at $E_{\text{app}} = -0.660$ V. This indicated a fully reversible oxidation process and the stable oxidized product during the experiment as predicted from the CV of **Fc-cnq**.

In the experiments, a series of potentials was applied to the optically transparent thin-layer cell in CH_3CN , and individual spectra were measured after equilibrium was attained at each potential as monitored by current decay to a small, essentially zero value. Figure 4 (potential-resolved spectra) shows the

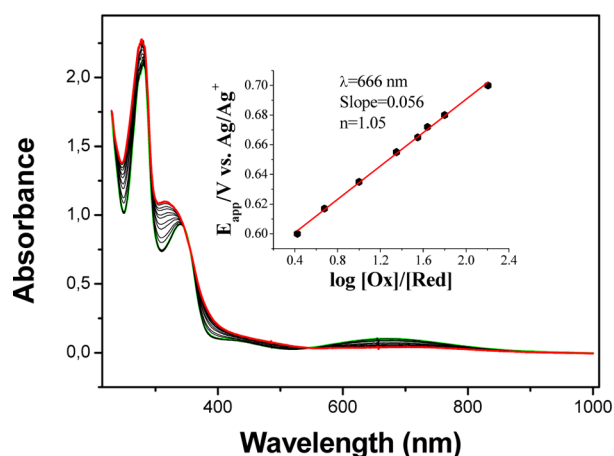


Figure 4. Potential-resolved UV-vis spectral changes of **Fc-cnq** during the oxidation process in CH_3CN solution containing 0.2 M TBAP where the inset shows the plot of E_{app} vs $\log[\text{O}]/[\text{R}]$.

result. The changes in the absorbance at a given wavelength (666 nm) can be related to the concentration ratio of oxidized to reduced species using eq 1^{82,86}

$$[\text{O}]/[\text{R}] = (A_i - A_0)/(A_f - A_i) \quad (1)$$

Here A_i is the absorbance of the mixture of oxidized and reduced forms, A_f is the absorbance of the totally oxidized form, and A_0 is the absorbance of the totally reduced form. The Nernst equation

$$E_{\text{app}} = E_{1/2} - (0.059/n) \log([\text{O}]/[\text{R}]) \quad (2)$$

indicates that a plot of E_{app} vs $\log[\text{O}]/[\text{R}]$ should be linear with a slope of $0.059/n$ V, assuming Nernstian reversibility. The number of the transferred electron for the oxidation process in the experiment was found as 1.05 (slope = 0.056 V, correlation coefficient = 0.998 for plot) (Figure 4, inset).

Effect of Water on the Redox Processes of Ferrocenyl Naphthoquinone Fused Crown Ether (Fc-cnq). At the initial stage of this experiment, the water content of the dried CH_3CN was determined by Karl Fischer (KF) coulometric titration,⁵⁷ and found as 0.0011 M. It was observed that this value raised to 0.051 M after the solution containing **Fc-cnq**, TBAP, and electrodes in the electrochemical cell (all of which were also conveniently dried before addition as described in the Experimental Section) was deoxygenated by a stream of high purity argon for 35 min to almost remove dissolved free oxygen in the solvent, thereby obtaining optimal standard redox potentials of **Fc-cnq**, especially for the dianion Fc-cnq^{2-} . It is noticed that the trace amount of free oxygen in the solvent may affect the standard redox potentials of the $\text{Fc-scncq}^{\bullet-}/\text{Fc-cnq}^{2-}$ process. Therefore, the purging time of the argon is prolonged to 35 min.

Figure 5 exhibits CVs of **Fc-cnq** before (black solid line, containing 0.051 M water determined by Karl Fischer coulometric titration) and after sequential addition of water in CH_3CN . The red solid line corresponds to the CV of **Fc-cnq** at a water concentration of 1.22 M water in CH_3CN . As seen from these CVs, the first and second reduction waves of $\text{Fc-scncq}^{\bullet-}/\text{Fc-cnq}^{2-}$ and $\text{Fc-cnq}/\text{Fc-scncq}^{\bullet-}$ pairs are shifted to more positive potential values with increasing water concentration. These results were attributed to the stabilization by the hydrogen bonding of mono- and dianion reduction products ($\text{Fc-scncq}^{\bullet-}$ and Fc-cnq^{2-}) as described by Gupta

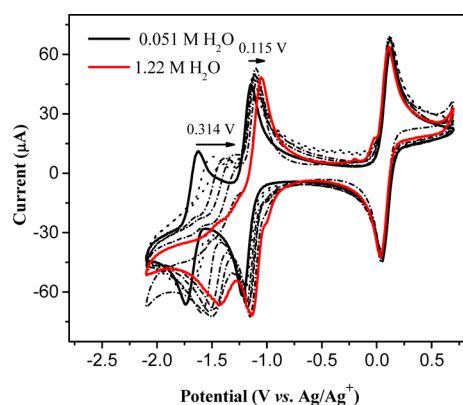


Figure 5. CVs of **Fc-cnq** in CH_3CN solution containing 0.2 M $n\text{-Bu}_4\text{NClO}_4$. Solid black line, before deliberate addition of water into the solution (0.051 M before starting the experiment); dotted black line, sequential addition of water into the solution; red line, final addition of water into the solution (1.22 M). Concentration of **Fc-cnq** = 5.0×10^{-3} M; scan rate = 0.100 V s^{-1} ; working electrode: glassy carbon disk electrode (3.0 mm diameter). In each step, the water content in the solution was accurately determined by KF titration.

and Linschitz,⁸⁷ Webster and co-workers,^{51,52} and others.^{35,36,50,65–68,88–92} The second reduction wave (Fc-cnq^{2-}) has no loss of reversibility by the addition of at least a water concentration of 1.22 M, but the process no longer keeps its reversibility at more water concentration probably due to the adsorption effects.^{51,52,80} Therefore, the data collection was stopped after higher water concentration >1.22 M. On the other hand, the first reduction and oxidation processes retained their reversibility at higher water concentration.

In addition, by the addition of water into the solution, no change was observed for the cathodic or anodic peak currents and the $E_{1/2}^{(\text{Fc})}$ value for the ($\text{Fc}^+-\text{cnq}/\text{Fc-cnq}$) process, which showed that the reversibility and stability of the ($\text{Fc}^+-\text{cnq}/\text{Fc-cnq}$) process were continued in spite of an increasing amount of water during the experiment. The plots of the $E_{1/2}$ values with varying water content in CH_3CN are shown in Figure 6. The $E_{1/2}^{(2)}$ value is more positively shifted (0.314 V) than the $E_{1/2}^{(1)}$ values (0.115 V) in the presence of the same amount of water (1.22 M) because the doubly reduced dianionic product (Fc-cnq^{2-}) having a highly negative charge over the carbonyl oxygen atom strongly favors the hydrogen-

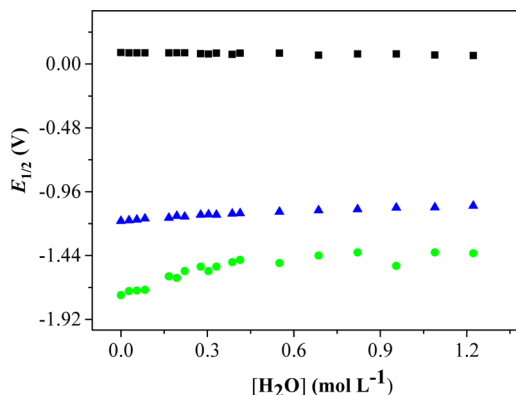
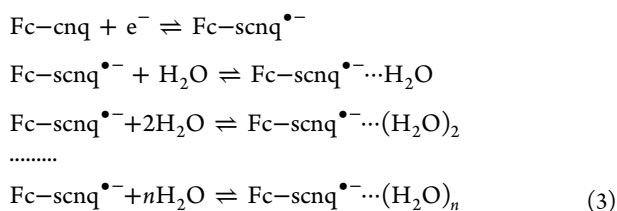


Figure 6. Plots of $E_{1/2}$ of the first reduction (blue triangle), the second reduction (green circle), and the oxidation (black square) waves vs water content of the solvent during the experiment; the concentration of **Fc-cnq** is 5.0×10^{-3} M.

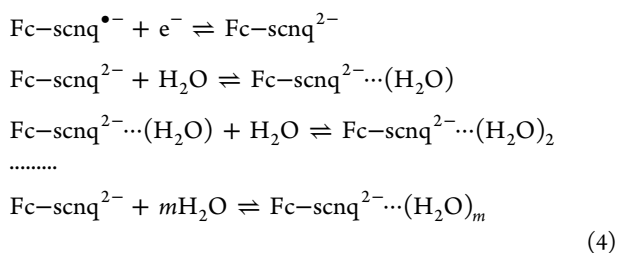
bonded forms with water molecules.⁸⁷ However, it is a great advantage that the $E^{(\text{Fc})}_{1/2}$ value for the $(\text{Fc}^+ - \text{cnq}/\text{Fc} - \text{cnq})$ process shows no change depending on varying concentration of water, which has been evaluated for the first time as an inner potential reference for accurate voltammetric determination of water content in the solvent. This behavior is very important for the cases when the voltammetric determination is based on the potential shift, where the reference potential selected must be stable for the accurate measurements. It is well-known that the Fc^+/Fc pair is used as the reference in organic media.⁹³

However, this reference is required at postcalibration. In this study, the half-wave potential ($E^{(\text{Fc})}_{1/2}$) corresponding to the $\text{Fc}^+ - \text{cnq}/\text{Fc} - \text{cnq}$ couple could be conveniently used as an internal potential reference without addition of ferrocene into the solution or considering $E^{(1)}_{1/2}$ values which may be changed depending on varying concentration of water or basicity of quinone molecules. As seen from Figures 5 and 6, the hydrogen-bonding interactions between water and the reduced species ($\text{Fc} - \text{snq}^{\bullet-}$ and $\text{Fc} - \text{cnq}^{2-}$) are redox-dependent. For the first and second reduction processes, the average number of water molecules (n and m) bound to the radical and the dianion species and equilibrium constants ($K^{(1)}_{\text{eq}}$ and $K^{(2)}_{\text{eq}}$) could be estimated by using eqs 11 and 14⁸⁷ which were herein rewritten for the ferrocenyl naphthoquinone **Fc-cnq** as the following

For the anion radical:



For the dianion:



where symbols n and m denote the average number of water molecules bound to the anion radical and dianion products, respectively. The equilibrium constants for eqs 3 and 4 can be written as

$$\begin{aligned}K^{(1)}_{\text{eq}} &= \frac{[\text{Fc-scnq}^{\bullet-} \cdots (\text{H}_2\text{O})_n]}{[\text{Fc-scnq}^{\bullet-}][\text{H}_2\text{O}]^n} \\ K^{(2)}_{\text{eq}} &= \frac{[\text{Fc-scnq}^{2-} \cdots (\text{H}_2\text{O})_m]}{[\text{Fc-scnq}^{2-}][\text{H}_2\text{O}]^m}\end{aligned}\quad (5)$$

The total concentration of anion radical formed in the reduction process is given by

$$[\text{Fc-scnq}^{\bullet-}]_{\text{total}} = [\text{Fc-scnq}^{\bullet-}] + [\text{Fc-scnq}^{\bullet-} \cdots (\text{H}_2\text{O})_n]\quad (6)$$

This is expressed in terms of the equilibrium constant $K^{(1)}_{\text{eq}}$ (in eq 5) as follows:

$$[\text{Fc-scnq}^{\bullet-}]_{\text{total}} = [\text{Fc-scnq}^{\bullet-}] \times (1 + K^{(1)}_{\text{eq}}[\text{H}_2\text{O}]^n)\quad (7)$$

The electrochemical reactions are reversible in our processes. The Nernst equation for the $\text{Fc-cnq}/\text{Fc-scnq}^{\bullet-}$ redox couple can be written as

$$E^{(1)} = E^{0(1)} + \frac{2.303RT}{nF} \log \left(\frac{[\text{Fc-cnq}]}{[\text{Fc-scnq}^{\bullet-}]}\right)\quad (8)$$

where $E^{0(1)}$ is the standard redox potential of the $\text{Fc-cnq}/\text{Fc-scnq}^{\bullet-}$ redox couple in the absence of water in solution, $E^{(1)}$ is the effective redox potential when water is present in solvent, R is the molar gas constant ($8.3145 \text{ J mol}^{-1} \text{ K}^{-1}$), T is the temperature (in Kelvin), n is the number of electrons transferred (here, $n = 1$), and F is the Faraday constant (96485 C mol^{-1}). Inserting eq 7 into eq 8, the following equation will be given

$$E^{(1)} = E^{0(1)} + \frac{2.303RT}{nF} \log \left(\frac{[\text{Fc-cnq}]}{[\text{Fc-scnq}^{\bullet-}]_{\text{total}}} \times (1 + K^{(1)}_{\text{eq}}[\text{H}_2\text{O}]^n) \right)\quad (9)$$

where $[\text{H}_2\text{O}]$ is the concentration of water added into the solution.

At the half-wave potential, the total concentrations of the oxidant and reductant are equal ($[\text{Fc-cnq}] = [\text{Fc-scnq}^{\bullet-}]$) and $E^{(1)}$ becomes $E^{(1)}_{1/2}$. Therefore, eq 9 becomes

$$E^{(1)}_{1/2} = E^{0(1)}_{1/2} + \frac{2.303RT}{F} \log(1 + K^{(1)}_{\text{eq}}[\text{H}_2\text{O}]^n)\quad (10)$$

If $K^{(1)}_{\text{eq}} \times [\text{H}_2\text{O}]^n \gg 1$ and the half-wave potential shift is denoted by $\Delta E^{(1)}_{1/2} = E^{(1)}_{1/2} - E^{0(1)}_{1/2}$, the above equation can be simplified as

$$\Delta E^{(1)}_{1/2} = \frac{2.303RT}{F} \log K^{(1)}_{\text{eq}} + \frac{2.303nRT}{F} \log([\text{H}_2\text{O}])\quad (11)$$

Figure 7 represents the plot of $\Delta E^{(1)}_{1/2}$ vs $\log[\text{H}_2\text{O}]$ which gives a straight line with a slope of $2.303nRT/F$, from which the value of n could be obtained as 1.6. The value of $K^{(1)}_{\text{eq}}$ was

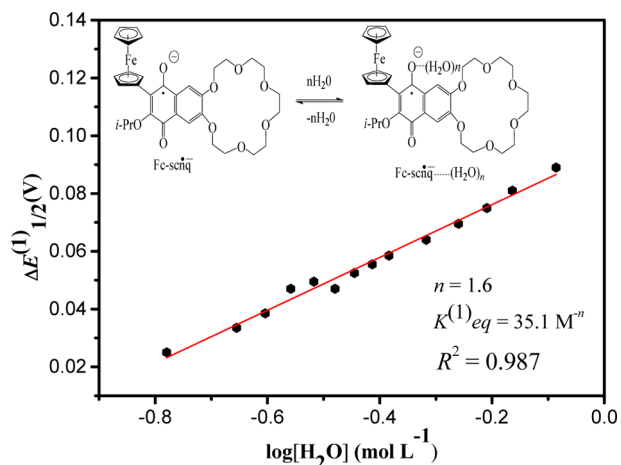


Figure 7. Plots of $\Delta E^{(1)}_{1/2}$ of the first reduction waves vs $\log[\text{H}_2\text{O}]$ during the experiment; the concentration of **Fc-cnq** is $5.0 \times 10^{-3} \text{ M}$.

calculated from the intercept of the plot, and found as 35.1 M^{-n} . The dianion formed in the case of the second reduction process proceeds in a similar way as the case of the anion radical. The total concentration for the dianion is

$$[\text{Fc-scnq}^{2-}]_{\text{total}} = [\text{Fc-scnq}^{2-}] + [\text{Fc-scnq}^{2-} \cdots (\text{H}_2\text{O})_m] \quad (12)$$

This is expressed in terms of the equilibrium constant $K_{\text{eq}}^{(2)}$ (in eq 5) as follows:

$$[\text{Fc-scnq}^{2-}]_{\text{total}} = [\text{Fc-scnq}^{2-}] \times (1 + K_{\text{eq}}^{(2)} [\text{H}_2\text{O}]^m) \quad (13)$$

Similar algebra was carried out to write the Nernst equation for the $\text{Fc-scnq}^{\bullet-}/\text{Fc-cnq}^{2-}$ redox pair. Finally, eq 14 has been written as follows:

$$E_{1/2}^{(2)} = E_{1/2}^{(0)(2)} + \frac{2.303RT}{F} \log \left(\frac{[\text{Fc-scnq}^{\bullet-}]}{[\text{Fc-cnq}^{2-}]} \right)$$

$$E_{1/2}^{(2)} = E_{1/2}^{(0)(2)} + \frac{2.303RT}{F} \log \left(\frac{(1 + K_{\text{eq}}^{(2)} [\text{H}_2\text{O}]^m)}{(1 + K_{\text{eq}}^{(1)} [\text{H}_2\text{O}]^n)} \right)$$

$$\Delta E_{1/2}^{(2)} = \frac{2.303RT}{F} \log \left(\frac{K_{\text{eq}}^{(2)}}{K_{\text{eq}}^{(1)}} \right) + \frac{2.303(m-n)RT}{F} \log([\text{H}_2\text{O}]) \quad (14)$$

Figure 8 shows the plot of $\Delta E_{1/2}^{(2)}$ vs $\log[\text{H}_2\text{O}]$ which gives a straight line with a slope of $2.303(m-n)RT/F$, from which

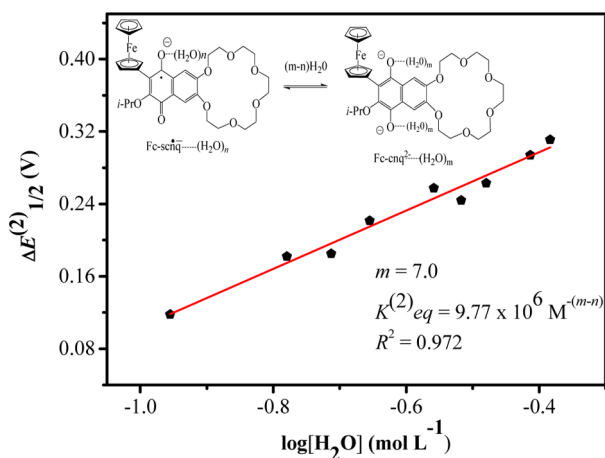


Figure 8. Plot of $\Delta E_{1/2}^{(2)}$ of the second reduction waves vs $\log[\text{H}_2\text{O}]$ during the experiment; the concentration of Fc-cnq is $5.0 \times 10^{-3} \text{ M}$.

the value of m could be obtained as 7.0. The value of $K_{\text{eq}}^{(2)}$ was calculated from the intercept of the plot, and found as $9.77 \times 10^6 \text{ M}^{-(m-n)}$. From eqs 11 and 14, one can readily deduce that the value of $(E_{1/2}^{(\text{Fc})} - E_{1/2}^{(2)})$ could be used for the determination of water content in CH_3CN solution. Figure 9 gives the plot of $(E_{1/2}^{(\text{Fc})} - E_{1/2}^{(2)})$ vs $\log[\text{H}_2\text{O}]$ (over low water concentration range). It could be seen that the graph is linear, enabling data to be fitted to a straight line equation of the form $y = -0.288x + 1.420$ ($R^2 = 0.985$). The calibrated water content range and potential range ($E_{1/2}^{(\text{Fc})} - E_{1/2}^{(2)}$) for CH_3CN were found to be 0.055–0.68 M and 1.792–1.473 V, respectively. Recording a single CV in the presence of Fc-cnq

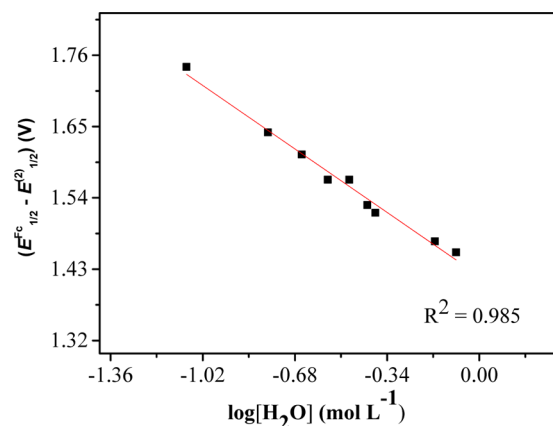


Figure 9. Plot of $(E_{1/2}^{(\text{Fc})} - E_{1/2}^{(2)})$ vs $\log[\text{H}_2\text{O}]$ during the experiment; the concentration of Fc-cnq is $5.0 \times 10^{-3} \text{ M}$.

and applying the straight line equation provides a simple and accurate method for determining the water content of CH_3CN during electrochemical experiments without ferrocene which is often used as an internal calibrant for the potential.

Effect of Weak and Strong Organic Acid on the Redox Processes of Ferrocenyl Naphthoquinone Fused Crown Ether (Fc-cnq). Figure 10 represents CVs of Fc-cnq

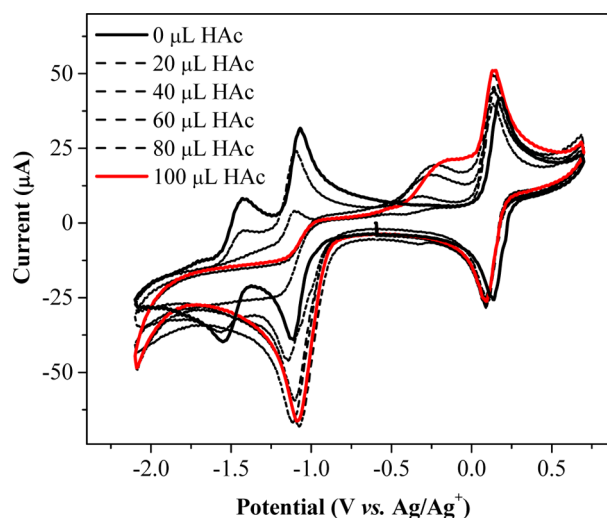


Figure 10. CVs of Fc-cnq in CH_3CN solution containing $0.2 \text{ M } n\text{-Bu}_4\text{NClO}_4$ during addition of AcOH into the solution. Scan rate = 0.100 V s^{-1} ; working electrode: glassy carbon disk electrode (3.0 mm diameter); concentration of Fc-cnq is $5.0 \times 10^{-3} \text{ M}$.

obtained by subsequent addition of $20 \mu\text{L}$ of acetic acid (AcOH) in CH_3CN at a scan rate of 0.100 V s^{-1} where the black solid line and red line are the CVs before and after the addition of AcOH , respectively. The reduction waves of $\text{Fc-scnq}^{\bullet-}$ and Fc-nq^{2-} products in acid free solution (black line) are replaced by a large cathodic wave appearing at $E_{\text{pc}} = -1.08 \text{ V}$ with a higher peak current and a positive potential shift, indicating probably formation of the hydroquinone product (Fc-hcnqH_2) by a sequence of two-electron and two-proton transfer.³⁷ The corresponding anodic wave observed at more positive potential ($E_{\text{pa}} = -0.151 \text{ V}$) was assigned to the reoxidation of the hydroquinone (Fc-hcnqH_2) to form the naphthoquinone Fc-cnq . The reversibility of the process corresponding to the ferrocenium/ferrocene (Fc^+/Fc)

ncq) was kept during the oxidation process in the presence of AcOH. A small negative potential shift observed for this wave ($\text{Fc}^+ - \text{cnq}/\text{Fc} - \text{cnq}$) can be attributed to the change of the polarity of the medium. The pathway was summarized in the direction of the green diagonal double arrows in Scheme 2. Similar behavior was also reported for different hydroquinones without a ferrocenyl moiety in weak acidic conditions.²⁰ No color and UV-vis spectral changes were observed upon addition of AcOH into the solution of the **Fc-cnq**, implying that **Fc-cnq** in the neutral state was not protonated in the presence of AcOH. However, addition of trifluoroacetic acid (TFA) to the solutions of **Fc-cnq** in CH_3CN resulted in a drastic color change from green to yellow, which was monitored by changing the UV-vis spectrum of **Fc-cnq** (Figure 11). As seen, the CT band at 666 and 339 nm ($n, \pi \rightarrow$

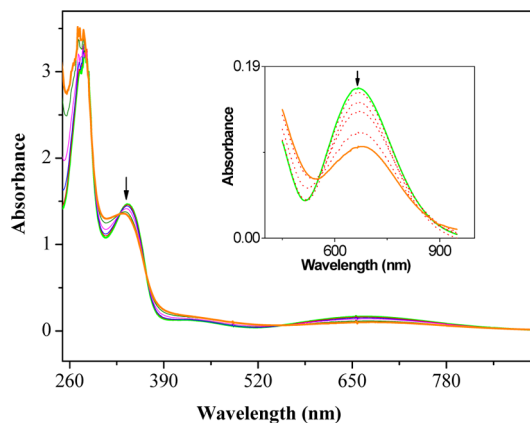


Figure 11. UV-vis spectra of **Fc-cnq** (green solid line) in CH_3CN , after addition of TFA (10 μL in 3 mL of solution) (orange line). The inset shows the magnified UV-vis spectra.

π^* transitions) decreased in intensity. These changes clearly indicate a chemical association between protons and clearly indicate a chemical association between proton and naphthoquinone groups. This approach and electron transfer mechanism were also verified with the CV technique. Figure 12 exhibits CVs of **Fc-cnq** obtained by subsequent addition of 10 μL of TFA in CH_3CN at a scan rate of 0.100 V s^{-1} where the black solid line and red line are the CVs in the absence of TFA and in the presence of 60 μL addition of TFA, respectively. The general electrochemical trend of **Fc-cnq** in TFA is almost similar to that of **Fc-cnq** in AcOH, but in TFA, the new wave based on the formation of the hydroquinone product (Fc-hcnqH_2) by a sequence of two-electron and one-proton transfer is evolved in the more positive potential ($E_{\text{pc}} = -0.781 \text{ V}$) than what is observed in AcOH. The UV-vis spectral and color changes in addition to the highly shifted potential value are directed to a new proposed mechanism for the electrochemistry of **Fc-cnq** in the TFA solution, which is presented in Scheme 3. According to the proposed mechanism, first, **Fc-cnq** is probably protonated at 1 or 4 positions of the naphthoquinone oxygen atom to give the ferrocenium semiquinone cation radical ($\text{Fc}^+ - \text{scnqH}^\bullet$). It accounts for an increase in the basicity of **Fc-cnq** by electron transfer from the donor ferrocene unit to the acceptor naphthoquinone ring in the molecule. Therefore, the cathodic wave in TFA, appearing at the more positive potential ($E_{\text{pc}} = -0.781 \text{ V}$) compared to that in AcOH ($E_{\text{pc}} = -1.08 \text{ V}$), is probably based on the hydroquinone (Fc-hcnqH_2) species, which is formed by two-

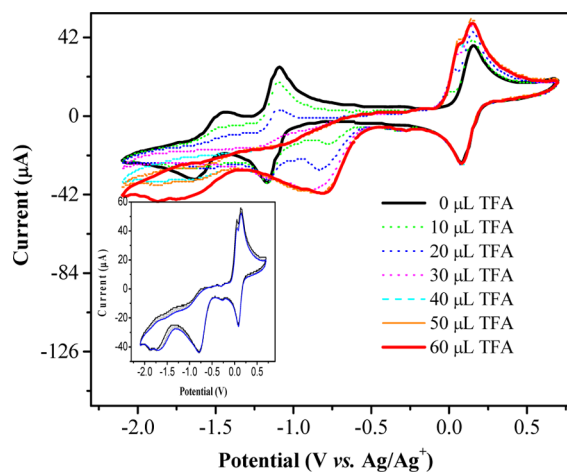


Figure 12. CVs of **Fc-cnq** in CH_3CN solution containing 0.2 M $n\text{-Bu}_4\text{NClO}_4$ during addition of TFA into the solution. Scan rate = 0.100 V s^{-1} ; working electrode: glassy carbon disk electrode (3.0 mm diameter); concentration of **Fc-cnq** = $5.0 \times 10^{-3} \text{ M}$. The inset shows the CV obtained after 10 cycles.

electron reduction coupled one-proton for $\text{Fc}^+ - \text{scnqH}^\bullet$. The corresponding anodic wave of Fc-hcnqH_2 was seen at 0.0590 V by losing two electrons and decoupled two protons, which was overlapped with the oxidation wave of ferrocene in the molecule. Almost no potential and current change were observed for the reversible one-electron oxidation process based on the ferrocenium/ferrocene ($\text{Fc}^+ - \text{ncq}/\text{Fc} - \text{ncq}$) species.

Metal Cation Binding Study of Ferrocenyl Naphthoquinone Fused Crown Ether (Fc-cnq**) with the UV-vis Titration Technique.** Figure 13 represents UV-vis spectra of **Fc-cnq** in the presence of an excess amount of alkali (Li^+ , Na^+ , K^+ , and Cs^+) and alkaline earth metal (Mg^{2+} , Ca^{2+} , and Ba^{2+}) perchlorates in CH_3CN . Their corresponding data are listed in Table 1. The spectrum of **Fc-cnq** (represented as a black line in Figure 12) exhibited a strong intensity band at 278 nm and two moderate intensity bands at 339 and 421 nm which are characteristic for naphthoquinone ($n, \pi \rightarrow \pi^*$) transitions. **Fc-cnq** also displayed a band at 666 nm which is a typical intramolecular CT transition taking place between the ferrocenyl donor and naphthoquinonyl acceptor center [$e\pi$ (HOMO-Fc) $\rightarrow e\pi^*$ (LUMO-cnq)].

This transition causes a green color of **Fc-cnq** and similar to the previously well-characterized intramolecular CT bands of ferrocene-DDQ (2,3-dichloro-5,6-dicyanobenzoquinone) [e_π (HOMO-Fc) $\rightarrow e_{\pi^*}$ (LUMO-DDQ)] and ferrocene-benzoquinone [e_π (HOMO-Fc) $\rightarrow e_{\pi^*}$ (LUMO-q) donor-acceptor dyads.^{37,94–97} The existence of the intramolecular CT transition was verified by the solvatochromic behavior of **Fc-cnq**. The electronic spectra of **Fc-cnq** were taken in several solvents with different solvating capabilities. The lower energy band distinctly shifted to higher energy in more highly solvating solvents, whereas the higher energy bands at the UV region showed little change in energy with solvent. Figure 6S represents a plot of band wavelength against Reichardt's overall solvation scale parameter [$E_T(30)$].⁹⁸

The alkali (Li^+ , Na^+ , K^+ , and Cs^+) and alkaline earth metal (Mg^{2+} , Ca^{2+} , and Ba^{2+}) cation binding abilities for **Fc-cnq** were studied by the UV-vis spectrophotometric titration technique in CH_3CN . In this way, the changes in the absorption intensity and the peak position, related with the CT band or the ($n, \pi \rightarrow$

Scheme 3. Electrochemical Reduction and Oxidation Mechanism for Fc–cnq in the Solution of CH₃CN after Addition of Strong Organic Acid (TFA)

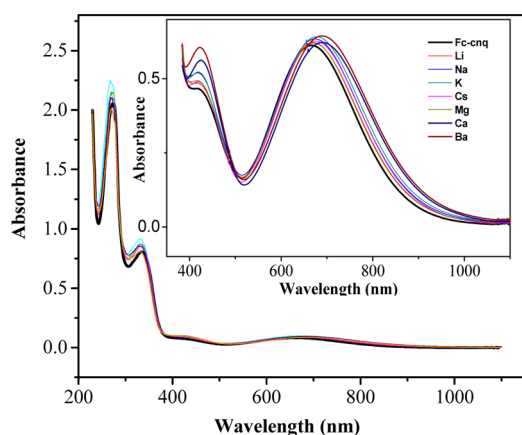
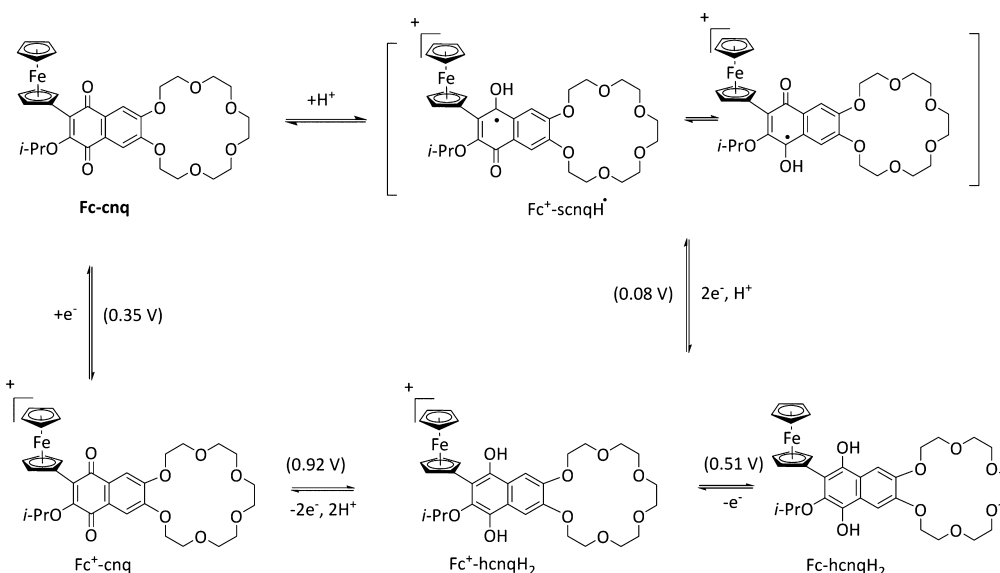
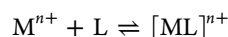


Figure 13. UV–vis spectra of Fc–cnq and its alkali (Li⁺, Na⁺, K⁺, and Cs⁺) and alkaline earth (Mg²⁺, Ca²⁺, and Ba²⁺) metal complexes in CH₃CN. Excess solid metal perchlorates were added into the solution of Fc–cnq (1.0 × 10^{−4} M). The spectra in the inset were taken in 1.0 × 10^{−3} M Fc–cnq.

π^*) bands, could be monitored during the metal cation binding experiment. As seen from Figure 13 and Table 1, both Ca²⁺ and Ba²⁺ ions exhibited considerable UV–vis spectral changes in absorption and peak position, although no other metal ions (Li⁺, Na⁺, K⁺, Cs⁺, and Mg²⁺) studied here gave rise to observable spectral changes in order to carry out a titration experiment in the same experimental conditions. The CT band at 666 nm was shifted by 21 nm to a longer wavelength for both Ba²⁺ and Ca²⁺ ions binding, while the absorption of the ($n, \pi \rightarrow \pi^*$) bands at 421 nm apparently increased in intensity. The extent of the shifts observed for the CT band may be listed in the order Ba²⁺ = Ca²⁺ > K⁺ > Cs⁺ > Na⁺ > Mg²⁺ > Li⁺ (Table 1), indicating that the best cation fitting into the cavity of the macrocyclic ring along with increasing charge density of cations are probably predominant on this observation.^{99–101} However, stoichiometry and complex formation constants (K_f) could be determined from the variations of absorbance at proper observation wavelengths (421 and 800 nm) which were chosen so that the variations were as large as possible. In the case of a

stoichiometry of 1:1, the formation constant K_f , which controls the equilibrium between the free ligand (L) that here defines Fc–cnq, and the complex [ML]^{*n*+},



and can be written as

$$K_f = \frac{[ML]^{n+}}{[M^{n+}][L]}$$

In a study conducted by Valeur,^{102,103} K_f values could be calculated utilizing the relationship between the UV–vis spectral changes and the concentration of the metal ion added for a related complexation reaction. Binding constants for 1:1 complexation were obtained by a nonlinear least-squares fit of the absorbance (X) vs the concentration of the metal ion added [M^{n+}] according to eq 13

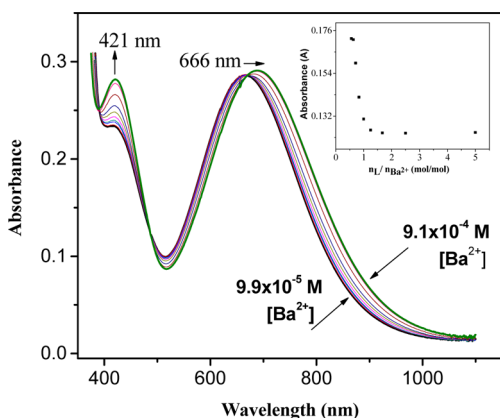
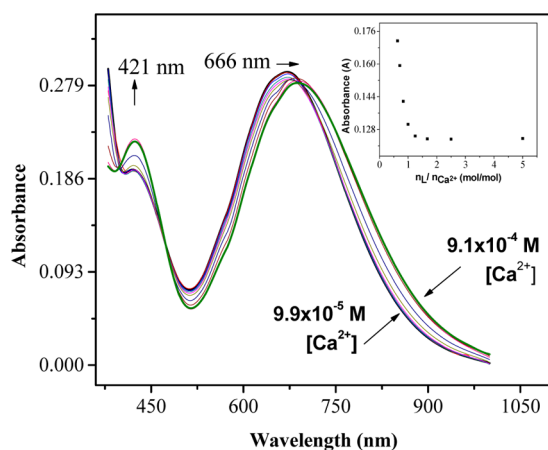
$$X = X_0 + \frac{X_{\text{lim}} - X_0}{2c_0} [c_0 + c_M + 1/K_s - [(c_0 + c_M + 1/K_s)^2 - 4c_0c_M]^{1/2}] \quad (15)$$

where X_0 and X are the absorbances of the complexes at a selected wavelength in the absence and presence of the metal cation, respectively, c_0 is the total concentration of the complex, [ML]^{*n*+}, c_M is the concentration of the metal cation [M^{n+}], and X_{lim} is the limiting value of the absorbance in the presence of excess metal ion. Figures 14 and 15 showed the UV–vis spectral changes observed for Fc–cnq upon subsequent addition of 10 μ L of Ba²⁺ and Ca²⁺ ions (concentration range: 9.9 × 10^{−5} to 9.1 × 10^{−4} M) in CH₃CN where insets were the plots of absorbance vs the mole ratio of the ligand to metal ions at 800 nm. It was clearly seen that the absorption for the CT band or the ($n, \pi \rightarrow \pi^*$) bands at 800 and 421 nm gradually increased with increasing concentration of Ba²⁺ and Ca²⁺ ions added into the solution of 1.0 × 10^{−4} M Fc–cnq in CH₃CN. It was evaluated from the inset graphs that the complex formation reactions displayed a stoichiometry of 1:1 in the case of Ba²⁺ and Ca²⁺ ions. The same result was observed from the plots of absorbance vs the mole ratio of the ligand to

Table 1. UV–vis Data and K_f Values of Fc–cnq in the Absence and Presence of Alkali (Li^+ , Na^+ , K^+ , and Cs^+) and Alkaline Earth Metal (Mg^{2+} , Ca^{2+} , and Ba^{2+}) Ions at 25.00 ± 0.02 °C in CH_3CN ^a

	diameter (Å)	charge density q (Å ⁻¹)	λ_{max} (nm) (log ϵ) (n, $\pi \rightarrow \pi^*$)			^{CT} λ_{max} (nm) (log ϵ) (HOMO \rightarrow LUMO) ($e_\pi \rightarrow e_\pi^*$)	formation constant log K_f
Fc–cnq	2.68–2.86 ^b		278 (4.21)	339 (3.81)	421 (2.67)	666 (2.79)	
Li ⁺	1.36	1.47	276 (4.23)	338 (3.84)	418 (2.69)	671 (2.79)	^c
Na ⁺	1.94	1.03	272 (4.26)	337 (3.86)	418 (2.72)	673 (2.80)	4.82 ^d
K ⁺	2.66	0.75	274 (4.23)	336 (3.84)	418 (2.72)	678 (2.81)	5.02 ^d
Cs ⁺	3.40	0.59	275 (4.24)	337 (3.84)	421 (2.69)	674 (2.80)	^c
Mg ⁺	1.32	3.03	274 (4.23)	337 (3.81)	417 (2.69)	672 (2.79)	^c
Ca ²⁺	1.98	2.02	269 (4.23)	331 (3.84)	421 (2.75)	687 (2.79)	4.91
Ba ²⁺	2.68	1.49	270 (4.21)	331 (3.81)	421 (2.78)	687 (2.81)	5.02

^a λ_{max} absorption maximum; ϵ , molar absorption coefficient; K_f , formation constant. ^bCavity size of 18-crown-6. ^c K_f could not be determined. ^d K_f was estimated by the conductometric technique in CH_3CN .

**Figure 14.** UV–vis spectral titration of Fc–cnq upon addition of aliquots of $\text{Ba}(\text{ClO}_4)_2$ in CH_3CN . The inset shows a plot of absorbance vs $n_L/n_{\text{Ca}^{2+}}$ (mol/mol). Concentration of Fc–cnq = 1.0×10^{-4} M.**Figure 15.** UV–vis spectral titration of Fc–cnq upon addition of aliquots of $\text{Ca}(\text{ClO}_4)_2$ in CH_3CN . The inset shows a plot of absorbance vs $n_L/n_{\text{Ca}^{2+}}$ (mol/mol). Concentration of Fc–cnq = 1.0×10^{-4} M.

metal ions at 421 nm (Figures 7S and 8S). The plots of the absorbance vs $[\text{Ba}^{2+}]$ or $[\text{Ca}^{2+}]$ showed sigmoidal curves, which indicated that the cations bind to Fc–cnq in a cooperative manner, as shown in Figures 9S and Figure 10S. Evaluating the data obtained from Figures 14 and 15 at 421 and 800 nm, according to eq 15, K_f could thus be obtained by a nonlinear least-squares analysis of X vs c_M and converted into K_f as a logarithmic constant, which of Ba^{2+} and Ca^{2+} were given in Table 1. As expected, the K_f value (5.02) corresponding to the 1:1 complexation between Fc–cnq and Ba^{2+} is higher than that of Fc–cnq and Ca^{2+} (4.91), indicating that the more stable metal complex is formed with Ba^{2+} . It is probably due to having the most appropriate size of Ba^{2+} cations (2.68 Å)^{102,103} for the cavity of Fc–cnq (ring size of 18C6 \approx 2.68 Å)¹⁰⁴ which gives rise to it being symmetrically positioned in the plane of the macrocyclic crown ether unit and induces a more efficient interaction with six oxygen atoms in a ligand conformation without introducing large strains in the ring bonds.

On the other hand, the Li^+ , Na^+ , K^+ , Cs^+ , and Mg^{2+} ion binding abilities for Fc–cnq were also studied by the UV–vis spectrophotometric titration technique in the same experimental condition, but no considerable spectral changes were observed to evaluate the stoichiometry and K_f for the related metal ion binding. However, stoichiometry and K_f for these metal ions binding in CH_3CN were also carried out to determine conductometrically at 25.00 ± 0.02 as below.

Metal Ion Binding Study of Ferrocenyl Naphthoquinone Fused Crown Ether (Fc–cnq) with the Conductometric Technique. The conductivity at a constant salt concentration (1.0×10^{-4} M) was monitored while increasing the concentration of the macrocycle Fc–cnq in CH_3CN at 25.00 ± 0.02 °C. Takeda¹⁰⁵ proposed a calculation of the formation constant K_f based on conductivity measurements. A related formula is given below:

$$K_f = (\Lambda_M - \Lambda) / (\Lambda - \Lambda_{ML}) [L] \quad (16)$$

$$[L] = [L]_t - [M]_t (\Lambda_M - \Lambda) / (\Lambda_M - \Lambda_{ML}) \quad (17)$$

The letters M, ML, and L symbolize metal perchlorate, complex, and ligand **Fc-cnq**, respectively. The measured conductivity values are denominated as $\mu\text{S}/\text{cm}$, and the formula is converted into the molar conductivity form and denominated as $\text{S}\cdot\text{cm}^2/\text{mol}$. By using conductivity values, it is possible to calculate the concentrations of the species in the environment and formation constant. According to the relevant formula, the nonlinear relationship is concerned between $[\text{L}]$ and $(\Lambda_{\text{M}} - \Lambda)/(\Lambda - \Lambda_{\text{ML}})$. Plots of the molar conductance (Λ) vs $[\text{L}]_t/[\text{M}]_t$ ratio obtained from our conductivity experiments for Ba^{2+} , Ca^{2+} , Na^+ , and K^+ cations in CH_3CN are shown in Figures 16,

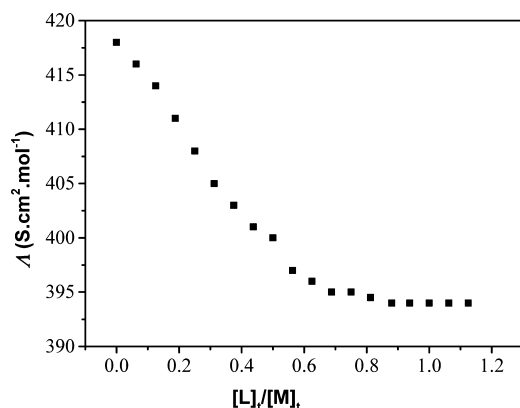


Figure 16. Plot of Λ vs $[\text{L}]_t/[\text{M}]_t$ for complexation of **Fc-cnq** and $\text{Ba}(\text{ClO}_4)_2$ in CH_3CN at 25.00 ± 0.02 °C. Concentration of **Fc-cnq** = 1.0×10^{-4} M.

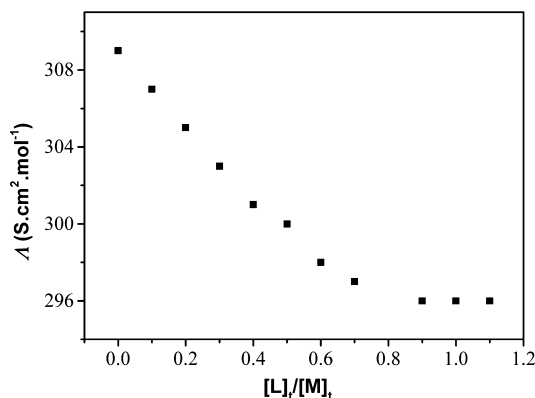


Figure 17. Plot of Λ vs $[\text{L}]_t/[\text{M}]_t$ for complexation of **Fc-cnq** and $\text{Ca}(\text{ClO}_4)_2$ in CH_3CN at 25.00 ± 0.02 °C. Concentration of **Fc-cnq** = 1.0×10^{-4} M.

17 and Figures 11S, 12S, respectively. As it is seen from the figures, the slopes change sharply at the point where the ligand to cation mole ratio is close to 1, emphasizing the formation of a relatively stable 1:1 complex between **Fc-cnq** and Na^+ , K^+ , Ca^{2+} , and Ba^{2+} ions.

In our calculations, K_f constants were found to be exponential, and calculated for each of the complexations, which were listed as $\log K_f$ in Table 1. $\log K_f$ constants of Ca^{2+} and Ba^{2+} cations calculated from conductometric measurements were in accord with those from the UV–vis titration technique mentioned above. As seen from Table 1, $\log K_f$ constants (5.02) for K^+ binding are the same as those for Ba^{2+} in view of their almost having the same size. In the metal ion binding study, the

ligand **Fc-cnq** to cation mole ratio and K_f constants for Li^+ , Cs^+ , and Mg^{2+} cations could not be calculated because the molar conductance data obtained in the presence of Li^+ , Cs^+ , and Mg^{2+} cations fluctuated as the increasing concentration of the macrocycle **Fc-cnq** in CH_3CN , probably due to partly unstable complex formations with these cations. It is well-known that the Li^+ and Mg^{2+} cations are too small with respect to the size of the macrocyclic cavity (18C6), and possibly only some of the oxygen atoms coordinate effectively to the Li^+ and Mg^{2+} cations.^{30,99–101} Additionally, the distances and orientation of the electrons of the donor atoms on the macrocycle unit of **Fc-cnq** could not permit the best position for the coordination to Li^+ and Mg^{2+} cations. Moreover, Li^+ and Mg^{2+} cations with the higher solvation energy cause unstable complexes. On the other hand, Cs^+ cations are too large to be accommodated into the cavity of the molecule; thus, Cs^+ cations probably located above the plane are not interacting as strongly with the oxygen atoms to form a stable complex as the Ca^{2+} or Ba^{2+} cations.^{30,99–101}

Theoretical Calculations. The electronic and optical properties of the **Fc-cnq** molecule have been theoretically investigated by means of density functional theory (DFT) and time-dependent DFT (TDDFT) calculations at the molecular level. The shape of the frontier molecular orbitals and their energies derived from TDDFT calculation in the acetonitrile solution are shown in Figure 18. The HOMO, HOMO–1, and HOMO–2 are localized on the ferrocenyl Fe (II) atom, while

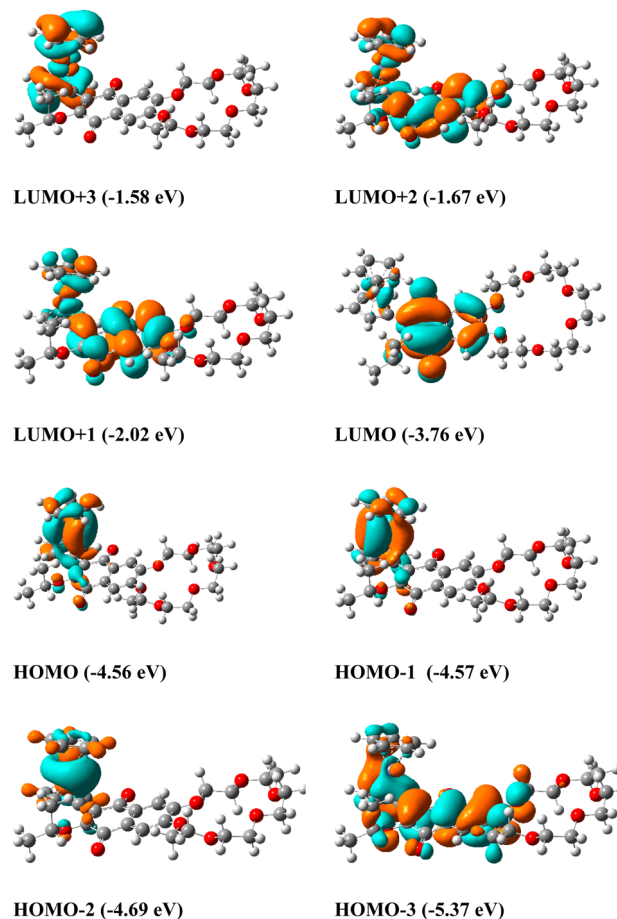


Figure 18. DFT-calculated frontier orbitals of **Fc-cnq** with molecular orbital energies.

Table 2. Calculated Optical Transitions and Their Character

exp. max. (nm)	wavelength (nm)	osc. strength	major contributions	character
666	1179.22	0.0485	H - 1 → LUMO (41%), HOMO → LUMO (22%)	CT
	515.88	0.0283	H - 8 → LUMO (36%), H - 4 → LUMO (38%)	
	501.89	0.012	H - 9 → LUMO (49%), H - 8 → LUMO (36%)	
	495.69	0.0209	H - 9 → LUMO (45%), H - 8 → LUMO (18%)	
	475.37	0.0609	H - 1 → L + 1 (48%), HOMO → L + 1 (17%)	
	462.00	0.0206	H - 2 → L + 1 (94%)	
421	433.06	0.0389	H - 12 → LUMO (52%), HOMO → L + 2 (20%)	n, $\pi \rightarrow \pi^*$
	428.00	0.0343	H - 1 → L + 2 (29%), HOMO → L + 2 (19%)	
	417.22	0.0168	H - 13 → LUMO (82%)	
	371.51	0.0113	H - 1 → L + 4 (47%), HOMO → L + 3 (17%)	
339	355.10	0.021	H - 15 → LUMO (84%)	n, $\pi \rightarrow \pi^*$
	352.30	0.0885	H - 3 → L + 1 (29%), H - 2 → L + 4 (37%)	
	344.70	0.2431	H - 3 → L + 1 (44%), H - 2 → L + 4 (23%)	CT
	340.01	0.0697	H - 3 → L + 3 (24%), H - 1 → L + 4 (14%)	
	332.37	0.0259	H - 2 → L + 4 (20%), H - 1 → L + 4 (19%)	
	323.61	0.0102	H - 3 → L + 2 (14%), H - 3 → L + 3 (53%)	
	320.50	0.0538	H - 4 → L + 1 (47%), H - 3 → L + 2 (29%)	
	318.88	0.0116	H - 5 → L + 1 (82%)	
	311.89	0.0105	H - 6 → L + 1 (91%)	
278	309.09	0.0112	H - 18 → LUMO (19%), H - 16 → LUMO (64%)	n, $\pi \rightarrow \pi^*$
	302.35	0.0788	H - 8 → L + 1 (63%)	
	297.83	0.0599	H - 8 → L + 1 (30%), H - 4 → L + 1 (18%)	
	286.48	0.0145	H - 1 → L + 5 (37%)	

the LUMO is predominately localized over the naphthoquinone moiety of the molecule. The Fc characteristic of HOMO and the naphthoquinone characteristic of LUMO show that the HOMO, HOMO-1, and HOMO-2 to LUMO absorption transitions exhibit intramolecular charge-transfer (CT) character, while the HOMO-3 to LUMO, LUMO+1, and LUMO+2 absorption transitions dominantly between the naphthoquinone characteristic orbitals suggest that these transitions are of $\pi \rightarrow \pi^*$ character. The experimentally obtained broad band at 666 nm is attributed as intramolecular charge transfer, while the other observed bands are mainly interpreted as $\pi \rightarrow \pi^*$ transitions according to theoretical calculations. The calculated optical transitions are given in Table 2. The calculated HOMO-LUMO gap (E_g) is 0.8 eV, which is lower than from the values derived from the experimentally obtained electrochemical and optical band gap, since only the ground state was taken into consideration in the molecular orbital calculation.

CONCLUSIONS

In this study, a novel multifunctional ferrocenyl naphthoquinone fused crown ether (benzo-18-crown-6) **Fc-cnq** has been synthesized via thermal rearrangement of intermediate ferrocenyl-substituted 4-hydroxy-4-(benzoyl-18-crown-6)-cyclobutenone (**3**) obtained from reaction of 3-ferrocenyl-4-isopropoxy-3-cyclobutene-1,2-dione (**1**) with lithio-benzo-18-crown-6 ether (**2**) in tetrahydrofuran (THF) at -78°C under nitrogen. The designed triad **Fc-cnq** has been broadly exploited for multisensor applications in this paper. First, it was seen that **Fc-cnq** was redox-dependent in the presence of water in the model aprotic organic solvent (CH_3CN), which enabled us to accurately determine a trace amount of water in

this solvent on the basis of hydrogen-bonding interactions between water and the electrochemically reduced species (**Fc-cnq**²⁻). In our study, the potential separation between the second reduction of the naphthoquinone ring and the oxidation processes of the ferrocene unit for **Fc-cnq** was for the first time applied for voltammetric determination of a trace amount of water in CH_3CN where the oxidation potential of ferrocene remained stable as water was added into the solution. Hence, it is a significant advantage that the half-wave potential of the ferrocene unit in the molecule can be used as an internal reference potential to accurate water determination in the solvent. Second, the multifunctional molecule **Fc-cnq** was utilized as a selective metal sensor toward Ba^{2+} and Ca^{2+} cations in CH_3CN solution on the basis of the ion-dipole interactions between the macrocyclic ring and cations. These interactions cause the intramolecular charge-transfer (CT) transition between the ferrocenyl donor and naphthoquinonyl acceptor center [$e\pi$ (HOMO-Fc) $\rightarrow e\pi^*$ (LUMO-cnq)] to shift toward lower energy. Frontier molecular orbital analysis obtained from DFT calculations has supported the experimentally obtained donor-acceptor behavior of **Fc-cnq**. The optical transition character has been investigated using TD-DFT calculations. The HOMO-LUMO energy gaps of the **Fc-cnq** are in agreement with their experimental electrochemical and optical results. As a third application, we have also herein presented an electrochemical approach to understand electron and proton-coupled electron transfer of the ferrocenyl naphthoquinones **Fc-cnq** in nonaqueous solutions in the presence of weak and strong organic acids such as acetic acid (AcOH) and trifluoroacetic acid (TFA), indicating that the multifunctional molecule **Fc-cnq** may also be utilized as a pH sensor.

■ ASSOCIATED CONTENT

■ Supporting Information

The Supporting Information is available free of charge on the ACS Publications website at DOI: 10.1021/acs.jpcc.5b06590.

Thermal rearrangement of ferrocenyl-substituted 4-hydroxy-4-(benzoyl-18-crown-6)cyclobutenone (**3**), FT-IR, ^1H and ^{13}C NMR, and HRMS spectra of **Fc-cnq**, plot of Reichardt's overall solvation scale against band wavelength for the lowest energy transition of **Fc-cnq** in a variety of solvents, the plots of absorbance vs $n_{\text{H}}/n_{\text{Ba}}^{2+}$ or $n_{\text{H}}/n_{\text{Ca}}^{2+}$, sigmoidal curves for **Fc-cnq**, $[\text{Ba}^{2+}]$ or $[\text{Ca}^{2+}]$ vs absorbance, and plot of Λ vs $[\text{L}]/[\text{M}]_{\text{t}}$ for complexation of **Fc-cnq** and NaClO_4 or KClO_4 in CH_3CN (PDF)

■ AUTHOR INFORMATION

Corresponding Author

*Phone: +90 212 2856831. Fax: +90 212 2856386. E-mail: iyilmaz@itu.edu.tr.

Notes

The authors declare no competing financial interest.

■ ACKNOWLEDGMENTS

This work was supported by The Scientific and Technical Research Council of Turkey (TUBİTAK, Project no. 113Z309). The theoretical calculations reported in this paper were performed at TUBİTAK ULAKBİM, High Performance and Grid Computing Center (TRUBA Resources).

■ REFERENCES

- (1) Gömer-Romero, P.; Sanchez, C. *Functional Hybrid Materials*; Wiley-VCH: Weinheim, Germany, 2004.
- (2) Ouahab, L. *Multifunctional Molecular Materials*; Ouahab, L., Ed.; Pan Stanford Publishing Pte. Ltd.: Singapore, 2013.
- (3) Hiraga, H.; Miyasaka, H.; Nakata, K.; Kajiura, T.; Takaishi, S.; Oshima, Y.; Nojiri, H.; Yamashita, M. Hybrid Molecular Material Exhibiting Single-Molecule Magnet Behavior and Molecular Conductivity. *Inorg. Chem.* **2007**, *46*, 9661–9671.
- (4) Alexandropoulos, D. I.; Mukherjee, S.; Papatriantafyllopoulou, C.; Raptopoulou, C. P.; Psycharis, V.; Bekiri, V.; Christou, G.; Stamatatos, T. C. A New Family of Nonanuclear Lanthanide Clusters Displaying Magnetic and Optical Properties. *Inorg. Chem.* **2011**, *50*, 11276–11278.
- (5) Goswami, S.; Adhikary, A.; Jena, H. S.; Konar, S. Lanthanide Based Coordination Polymers Chill, Relax Under Magnetic Field and also Fluoresce. *Dalton Trans.* **2013**, *42*, 9813–9817.
- (6) Pointillart, F.; Guennic, B. L.; Golhen, S.; Cador, O.; Maury, O.; Ouahab, L. A Redox-active Luminescent Ytterbium Based Single Molecule Magnet. *Chem. Commun.* **2013**, *49*, 615–617.
- (7) Mazarakioti, E. C.; Poole, K. M.; Cunha-Silva, L.; Christou, G.; Stamatatos, T. C. A New Family of Ln₇ Clusters with an Ideal D_{3h} Metal-Centered Trigonal Prismatic Geometry, and SMM and Photoluminescence Behaviors. *Dalton Trans.* **2014**, *43*, 11456–11460.
- (8) Stich, M. I. J.; Fischer, L. H.; Wolfbeis, O. S. Multiple Fluorescent Chemical Sensing and Imaging. *Chem. Soc. Rev.* **2010**, *39*, 3102–3114.
- (9) Borchert, N. B.; Ponomarev, G. V.; Kerry, J. P.; Papkovsky, D. B. O(2)/pH Multisensor Based on One Phosphorescent Dye. *Anal. Chem.* **2011**, *83*, 18–22.
- (10) Tian, Y.; Shumway, B. R.; Youngbull, A. C.; Li, Y.; Jen, A. K.; Johnson, R. H.; Meldrum, D. R. Dually Fluorescent Sensing of pH and Dissolved Oxygen Using a Membrane Made from Polymerizable Sensing Monomers. *Sens. Actuators, B* **2010**, *147*, 714–722.
- (11) Colacot, T. J. A Concise Update on The Applications of Chiral Ferrocenyl Phosphines in Homogeneous Catalysis Leading to Organic Synthesis. *Chem. Rev.* **2003**, *103*, 3101–3118.
- (12) Štěpnička, P. *Ferrocenes: Ligands, Materials and Biomolecules*; John Wiley & Sons Ltd.: Chichester, U.K., 2008.
- (13) van Staveren, D. R.; Metzler-Nolte, N. Bioorganometallic Chemistry of Ferrocene. *Chem. Rev.* **2004**, *104*, 5931–85.
- (14) Winkler, J. R.; Gray, H. B. Electron Transfer in Ruthenium-Modified Proteins. *Chem. Rev.* **1992**, *92*, 369–379.
- (15) McLendon, G.; Hake, R. Interprotein Electron Transfer. *Chem. Rev.* **1992**, *92*, 481–490.
- (16) Isied, S. S.; Ogawa, M. Y.; Wishart, J. F. Peptide-Mediated Intramolecular Electron Transfer: Long-Range Distance Dependence. *Chem. Rev.* **1992**, *92*, 381–394.
- (17) Tollin, G. In *Electron Transfer in Chemistry*; Balzani, V., Ed.; Wiley-VCH: Weinheim, Germany, 2001; Vol. 4, p 202.
- (18) Costentin, C. Electrochemical Approach to the Mechanistic Study of Proton-coupled Electron Transfer. *Chem. Rev.* **2008**, *108*, 2145–79.
- (19) Swallow, A. J. In *Function of Quinones in Energy Conserving Systems*; Trumpover, B. L., Ed.; Academic Press: New York, 1982; Chapter 3.
- (20) Chambers, J. Q. In *The Chemistry of the Quinonoid Compounds*; Rappoport, Z.; Patai, Z., Eds.; J. Wiley & Sons: New York, 1988; Vol. II, Chapter 12, p 719.
- (21) Langdon-Jones, E. E.; Pope, S. J. A. The Coordination Chemistry of Substituted Anthraquinones: Developments and Applications. *Coord. Chem. Rev.* **2014**, *269*, 32–53.
- (22) Zhu, L.; Khairutdinov, R. F.; Cape, J. L.; Hurst, J. K. Photoregulated Transmembrane Charge Separation by Linked Spiropyran-Anthraquinone Molecules. *J. Am. Chem. Soc.* **2006**, *128*, 825–35.
- (23) Devaraj, S.; Saravanakumar, D.; Kandaswamy, M. Dual Chemosensing Properties of New Anthraquinone-based Receptors Toward Fluoride Ions. *Tetrahedron Lett.* **2007**, *48*, 3077–3081.
- (24) Ranyuk, E.; Douaihy, C. M.; Bessmertnykh, A.; Denat, F.; Averin, A.; Beletskaya, I.; Guilard, R. Diaminoanthraquinone-linked Polyazamacrocycles: Efficient and Simple Colorimetric Sensor for Lead Ion in Aqueous Solution. *Org. Lett.* **2009**, *11*, 987–90.
- (25) Beer, P. D.; Gale, P. A.; Chen, G. Z. Mechanisms of Electrochemical Recognition of Cations, Anions and Neutral Guest Species by Redox-Active Receptor Molecules. *Coord. Chem. Rev.* **1999**, *185–186*, 3–36.
- (26) Bolas, P. L.; Gómez-Kaifer, M.; Echegoyen, L. Electrochemistry of Supramolecular Systems. *Angew. Chem., Int. Ed.* **1998**, *37*, 216–247.
- (27) Pedersen, C. J. New Macrocyclic Polyethers. *J. Am. Chem. Soc.* **1970**, *92*, 391–394.
- (28) Pedersen, C. J. Crystalline Salt Complexes of Macrocyclic Polyethers. *J. Am. Chem. Soc.* **1970**, *92*, 386–391.
- (29) Pedersen, C. J. Cyclic Polyethers and Their Complexes with Metal Salts. *J. Am. Chem. Soc.* **1967**, *89*, 2495–2496.
- (30) Izatt, R. M.; Pawlak, K.; Bradshaw, J. S.; Bruening, R. L. Thermodynamic and Kinetic Data for Macrocyclic Interaction with Cations, Anions, and Neutral Molecules. *Chem. Rev.* **1995**, *95*, 2529–2586.
- (31) Fabre, B.; Simonet, J. Electroactive Polymers Containing Crown Ether or Polyether Ligands as Cation-Responsive Materials. *Coord. Chem. Rev.* **1998**, *178–180*, 1211–1250.
- (32) Steed, J. W.; Atwood, J. L. *Supramolecular Chemistry*; J. Wiley & Sons: Chichester, West Sussex, U.K., 2009.
- (33) Valeur, B.; Leray, I. Design Principles of Fluorescent Molecular Sensors for Cation Recognition. *Coord. Chem. Rev.* **2000**, *205*, 3–40.
- (34) Beer, P. D.; Hayes, E. J. Transition Metal and Organometallic Anion Complexation Agents. *Coord. Chem. Rev.* **2003**, *240*, 167–189.
- (35) Valeur, B.; Leray, I. Design Principles of Fluorescent Molecular Sensors for Cation Recognition. *Coord. Chem. Rev.* **2000**, *205*, 3–40.
- (36) Hamilton, G. R. C.; Sahoo, S. K.; Kamila, S.; Singh, N.; Kaur, N.; Hyland, B. W.; Callan, J. F. Optical Probes for The Detection of Protons, and Alkali and Alkaline Earth Metal Cations. *Chem. Soc. Rev.* **2015**, *44*, 4415–4432.

- (37) Yucel, B.; Sanli, B.; Soylemez, H.; Yilmaz, I. Synthesis and Electro-Spectroelectrochemistry of Ferrocenyl Naphthaquinones. *Tetrahedron* **2011**, *67*, 1406–1421.
- (38) Zora, M.; Yucel, B.; Acikalin, S. Synthesis of Ferrocenyl Quinones. *Tetrahedron Lett.* **2003**, *44*, 2237–2241.
- (39) Chan, K. S.; Zhang, H. Synthesis of Ferrocenyl Quinones by Benzannulation with Fischer Carbene Complexes. *Synth. Commun.* **1995**, *25*, 635–639.
- (40) Beer, P. D. Transition Metal and Organic Redox-Active Macrocycles Designed to Electrochemically Recognize Charged and Neutral Guest Species. *Adv. Inorg. Chem.*; Sykes, A. G., Ed.; Academic Press: San Diego, California, 1992; Vol. 39, pp 79–157.
- (41) Beer, P. D. Redox Responsive Macrocyclic Receptor Molecules Containing Transition Metal Redox Centres. *Chem. Soc. Rev.* **1989**, *18*, 409–450.
- (42) Grossel, M. C.; Hamilton, D. G.; Fuller, J. I.; Millan-Barios, E. Alkali-Metal Binding Properties of Simple Ferrocenyl- and Ruthenocenyl-Substituted Aza-Crown Ethers. *J. Chem. Soc., Dalton Trans.* **1997**, 3471–3477.
- (43) Tendero, M. J. L.; Benito, A.; Martinez-Manez, R.; Soto, J.; Paya, J.; Edwards, A. J.; Raithby, P. R. Tuning of The Electrochemical Recognition of Substrates as A Function of The Proton Concentration in Solution Using pH-Responsive Redox-Active Receptor Molecules. *J. Chem. Soc., Dalton Trans.* **1996**, 343–351.
- (44) Zhang, H.; Zhou, B.; Li, H.; Qu, D.-H.; Tian, H. A Ferrocene-Functionalized [2]Rotaxane with Two Fluorophores as Stoppers. *J. Org. Chem.* **2013**, *78*, 2091–2098.
- (45) Rahman, Md. A.; Kwon, N.-H.; Won, M.-S.; Hyun, M.-H.; Shim, Y.-B. Selective Binding of NH_4^+ by Redox-Active Crown Ethers: Application to a NH_4^+ Sensor. *Anal. Chem.* **2004**, *76*, 3660–3665.
- (46) Wolf, R. E.; Cooper, S. R. Redox-Active Crown Ethers: Molecules Designed to Couple Ion Binding With A Redox Reaction. *J. Am. Chem. Soc.* **1984**, *106*, 4646–4647.
- (47) Sugihara, K.; Kamiya, H.; Yamaguchi, M.; Kaneda, T.; Misumi, S. Synthetic Macrocyclic Ligands. III. Synthesis of A Quinone-Hydroquinone Redox System Incorporated With Complexing Ability Toward Cations. *Tetrahedron Lett.* **1981**, *22*, 1619–1622.
- (48) Bock, H.; Hierholzer, B.; Vögtle, F.; Hollmann, G. Radical Anion-Substituted Crown Ethers as Cages for Metal Cations. *Angew. Chem., Int. Ed. Engl.* **1984**, *23*, 57–58.
- (49) Rahman, M. A.; Won, M.-S.; Kwon, N.-H.; Yoon, J.-H.; Park, D.-S.; Shim, Y.-B. Water Sensor for a Nonaqueous Solvent with Poly(1,5-diaminonaphthalene) Nanofibers. *Anal. Chem.* **2008**, *80*, 5307–5311.
- (50) Zhang, L.; Zhou, H.; Li, X.; Lin, Y.; Yu, P.; Su, L.; Mao, L. Voltammetric Determination of Water With Inner Potential Reference and Variable Linear Range Based on Structure- and Redox-Controlable Hydrogen-Bonding Interaction Between Water And Quinones. *Electrochem. Commun.* **2009**, *11*, 808–811.
- (51) Hui, Y.; Chng, E. L. K.; Chng, C. Y. L.; Poh, H. L.; Webster, R. D. Hydrogen-Bonding Interactions between Water and the One- and Two-Electron-Reduced Forms of Vitamin K1: Applying Quinone Electrochemistry to Determine the Moisture Content of Non-Aqueous Solvents. *J. Am. Chem. Soc.* **2009**, *131*, 1523–1534.
- (52) Hui, Y.; Chng, E. L. K.; Chua, L. P.-L.; Liu, W. Z.; Webster, R. D. Voltammetric Method for Determining the Trace Moisture Content of Organic Solvents Based on Hydrogen-Bonding Interactions with Quinones. *Anal. Chem.* **2010**, *82*, 1928–1934.
- (53) Tessensohn, M. E.; Hirao, H.; Webster, R. D. Electrochemical Properties of Phenols and Quinones in Organic Solvents are Strongly Influenced by Hydrogen-Bonding with Water. *J. Phys. Chem. C* **2013**, *117*, 1081–1090.
- (54) Saraullo, A.; Martos, P. A.; Pawliszyn, J. Water Analysis by Solid Phase Microextraction Based on Physical Chemical Properties of the Coating. *Anal. Chem.* **1997**, *69*, 1992–1998.
- (55) Gupta, T.; van der Boom, M. E. Optical Sensing of Parts per Million Levels of Water in Organic Solvents Using Redox-Active Osmium Chromophore-Based Monolayers. *J. Am. Chem. Soc.* **2006**, *128*, 8400–8401.
- (56) Kuang, Q.; Lao, C.; Wang, Z. L.; Xie, Z.; Zheng, L. High-Sensitivity Humidity Sensor Based on a Single SnO_2 Nanowire. *J. Am. Chem. Soc.* **2007**, *129*, 6070–6071.
- (57) Scholz, E. *Karl Fischer Titration: Determination of Water*; Springer-Verlag: Berlin, 1984.
- (58) Bühlmann, P.; Pretsch, E.; Bakker, E. Carrier-Based Ion-Selective Electrodes and Bulk Optodes. 2. Ionophores for Potentiometric and Optical Sensors. *Chem. Rev.* **1998**, *98*, 1593–1688.
- (59) Xia, Z.; Badr, I. H. A.; Plummer, S. L.; Cullen, L.; Bachas, L. G. Synthesis and Evaluation of a Bis(crown ether) Ionophore with a Conformationally Constrained Bridge in Ion-Selective Electrodes. *Anal. Sci.* **1998**, *14*, 169–173.
- (60) Gokel, G. W.; Leevy, W. M.; Weber, M. E. Crown Ethers: Sensors for Ions and Molecular Scaffolds for Materials and Biological Models. *Chem. Rev.* **2004**, *104*, 2723–2750.
- (61) Laviron, E. Electrochemical Reactions with Protonations at Equilibrium: Part XIII. Experimental Study of The Homogeneous Electron Exchange in Quinone/Dihydroquinone Systems. *J. Electroanal. Chem. Interfacial Electrochem.* **1986**, *208*, 357–372.
- (62) Peover, M. E. In *Electroanalytical Chemistry*; Bard, A. J., Ed.; Dekker: New York, 1967; p 1.
- (63) Laviron, E. Electrochemical Reactions with Protonations at Equilibrium: Part XII. The $2e^-$, $2H^+$ Homogeneous Isotopic Electron Exchange Reaction (Nine-Member Square Scheme). *J. Electroanal. Chem. Interfacial Electrochem.* **1984**, *169*, 29–46.
- (64) Aguilar-Martínez, M.; Bautista-Martínez, J. A.; Macías-Ruvalcaba, N.; González, I.; Tovar, E.; Marín del Alizal, T.; Collera, O.; Cuevas, G. Molecular Structure of Substituted Phenylamine α -OMe- and α -OH-*p*-Benzoquinone Derivatives. Synthesis and Correlation of Spectroscopic, Electrochemical, and Theoretical Parameters. *J. Org. Chem.* **2001**, *66*, 8349–8363.
- (65) Ortiz, J. L.; Delgado, J.; Baeza, A.; González, I.; Sanabria, R.; Miranda, R. Control of The Electrochemical Reduction of Horminone by Ph Imposition in Acetonitrile. *J. Electroanal. Chem.* **1996**, *411*, 103–107.
- (66) Bautista-Martínez, J. A.; González, I.; Aguilar-Martínez, M. Influence of Acidity Level in Acetonitrile on Hammett–Zuman Type Correlations on The Reduction of A-Hydroxyquinones. *Electrochim. Acta* **2003**, *48*, 4239–4244.
- (67) Gómez, M.; González, F. J.; González, I. Intra and Intermolecular Hydrogen Bonding Effects in The Electrochemical Reduction of A-Phenolic-Naphthoquinones. *J. Electroanal. Chem.* **2005**, *578*, 193–202.
- (68) González, F. J. Cyclic Voltammetry of Two Analogue K-Group Vitamin Compounds in Dimethylsulfoxide. *Electroanalysis* **1998**, *10*, 638–642.
- (69) Lin, X. Q.; Kadish, K. M. Vacuum-Tight Thin-Layer Spectroelectrochemical Cell with A Doublet Platinum Gauze Working Electrode. *Anal. Chem.* **1985**, *57*, 1498–1501.
- (70) Frisch, M. J.; Trucks, G. W.; Schlegel, H. B.; Scuseria, G. E.; Robb, M. A.; Cheeseman, J. R.; Scalmani, G.; Barone, V.; Mennucci, B.; Petersson, G. A.; et al. *Gaussian 09*; Gaussian, Inc.: Wallingford, CT, 2009.
- (71) Hohenberg, P.; Kohn, W. Inhomogeneous Electron Gas. *Phys. Rev.* **1964**, *136*, B864–B871.
- (72) Kohn, W.; Sham, L. J. Self-Consistent Equations Including Exchange and Correlation Effects. *Phys. Rev.* **1965**, *140*, A1133–A1138.
- (73) Adamo, C.; Barone, V. Exchange Functionals With Improved Long-range Behavior and Adiabatic Connection Methods Without Adjustable Parameters: The mPW and mPW1PW Models. *J. Chem. Phys.* **1998**, *108*, 664–675.
- (74) Stratmann, R. E.; Scuseria, G. E.; Frisch, M. J. An Efficient Implementation of Time-Dependent Density-Functional Theory for the Calculation of Excitation Energies of Large Molecules. *J. Chem. Phys.* **1998**, *109*, 8218–8224.
- (75) Grimme, S. Semiempirical GGA-type Density Functional Constructed with A Long-Range Dispersion Correction. *J. Comput. Chem.* **2006**, *27*, 1787–1799.

- (76) Sun, P.; Xu, D. X.; Mándi, A.; Kurtán, T.; Li, T. J.; Schulz, B.; Zhang, W. Structure, Absolute Configuration, and Conformational Study of 12-Membered Macrolides from The Fungus *Dendrodochium* sp. Associated with The Sea Cucumber *Holothuria nobilis* Selenka. *J. Org. Chem.* **2013**, *78*, 7030–7047.
- (77) Mennucci, B.; Tomasi, J. Continuum Solvation Models: A New Approach to the Problem of Solute's Charge Distribution and Cavity Boundaries. *J. Chem. Phys.* **1997**, *106*, 5151–5158.
- (78) Aguilar-Aguilar, A.; Peña-Cabrera, E.; Liebeskind, L. S. Synthesis of Squaric Acid Ester-Containing Ferrocene Derivatives. *Arkivoc* **2004**, 156–162.
- (79) Ungaro, R.; El Haj, B.; Smid, J. Substituent Effects on The Stability of Cation Complexes of 4'-Substituted Monobenzo Crown Ethers. *J. Am. Chem. Soc.* **1976**, *98*, 5198–5202.
- (80) Staley, P. A.; Newell, C. M.; Pullman, D. P.; Smith, D. K. The Effect of Glassy Carbon Surface Oxides in Non-Aqueous Voltammetry: The Case of Quinones in Acetonitrile. *Anal. Chem.* **2014**, *86*, 10917–10924.
- (81) Bard, A. J.; Faulkner, L. R., Eds. *Electrochemical Methods: Fundamentals and Applications*, 2nd ed.; John Wiley & Sons: New York, 2001.
- (82) Yilmaz, I. In Situ Monitoring of Metallation of Metal-Free Phthalocyanine via UV-Vis and Steady-State Fluorescence Techniques. Thin-layer UV-Vis and Fluorescence Spectroelectrochemistry of A New Non-Aggregating and Electrochromic Manganese(3+) phthalocyanine. *New J. Chem.* **2008**, *32*, 37–46.
- (83) Yilmaz, I.; Arslan, S.; Guney, S.; Becerik, I. Synthesis, Electro-Spectroelectrochemical Characterization and Electrocatalytic Behavior Towards Dioxygen Reduction of A New Water-Soluble Cobalt Phthalocyanine Containing Naphthoxy-4-Sulfonic Acid Sodium Salt. *Electrochim. Acta* **2007**, *52*, 6611–6621.
- (84) Kadish, K. M.; Nakanishi, T.; Gürek, A.; Ahsen, V.; Yilmaz, I. Electrochemistry of a Double-Decker Lutetium(III) Phthalocyanine in Aqueous Media. The First Evidence for Five Reductions. *J. Phys. Chem. B* **2001**, *105*, 9817–9821.
- (85) Nakanishi, T.; Yilmaz, I.; Nakashima, N.; Kadish, K. M. Thermodynamic Study of Ion-Pairing Effects between Reduced Double-Decker Lutetium(III) Phthalocyanines and a Cationic Matrix. *J. Phys. Chem. B* **2003**, *107*, 12789–12796.
- (86) Yilmaz, I.; Nakanishi, T.; Gürek, A.; Kadish, K. M. Electrochemical and spectroscopic investigation of neutral, oxidized and reduced double-decker lutetium(III) phthalocyanines. *J. Porphyrins Phthalocyanines* **2003**, *7*, 227–238.
- (87) Gupta, N.; Linschitz, H. Hydrogen-Bonding and Protonation Effects in Electrochemistry of Quinones in Aprotic Solvents. *J. Am. Chem. Soc.* **1997**, *119*, 6384–6391.
- (88) Peover, M. E.; Davies, J. D. Reduction Potentials and Intermolecular Charge-Transfer Spectra of Organic Acceptor Molecules. Part 3.-Solvent Effects on *p*-Benzoquinones. *Trans. Faraday Soc.* **1964**, *60*, 476–478.
- (89) Umemoto, K. Studies of the Electrolytic Reduction Mechanism of Anthracene, Benzophenone and Anthraquinone by the Use of Polarography and Electron Spin Resonance Spectroscopy. *Bull. Chem. Soc. Jpn.* **1967**, *40*, 1058–1065.
- (90) Eggins, B. R. Interpretation of Electrochemical Reduction and Oxidation Waves of Quinone-Hydroquinone System In Acetonitrile. *J. Chem. Soc. D* **1969**, 1267–1268.
- (91) Laviron, E. Electrochemical Reactions with Protonations at Equilibrium: Part XIII. Experimental Study of The Homogeneous Electron Exchange in Quinone/Dihydroquinone Systems. *J. Electroanal. Chem. Interfacial Electrochem.* **1986**, *208*, 357–372.
- (92) Lehmann, M. W.; Evans, D. H. Anomalous Behavior in The Two-Step Reduction of Quinones in Acetonitrile. *J. Electroanal. Chem.* **2001**, *500*, 12–20.
- (93) Gagne, R. R.; Koval, C. A.; Lisensky, G. C. Ferrocene as An Internal Standard for Electrochemical Measurements. *Inorg. Chem.* **1980**, *19*, 2854–2855.
- (94) Colbran, S. B.; Lee, S. T.; Lonnon, D. G.; Maharaj, F. J. D.; McDonagh, A. M.; Walker, K. A.; Young, R. D. Covalently Linked Ferrocenyl Quinones: Proton-Dependent Redox Behavior and Charge Redistribution. *Organometallics* **2006**, *25*, 2216–2224.
- (95) Barlow, S.; Bunting, H. E.; Ringham, C.; Green, J. C.; Bublitz, G. U.; Boxer, S. G.; Perry, J. W.; Marder, S. R. Studies of the Electronic Structure of Metallocene-Based Second-Order Nonlinear Optical Dyes. *J. Am. Chem. Soc.* **1999**, *121*, 3715–3723.
- (96) Barlow, S.; O'Hare, D. Metal–Metal Interactions in Linked Metallocenes. *Chem. Rev.* **1997**, *97*, 637–670.
- (97) Gebert, E.; Reis, A. H.; Miller, J. S.; Rommelmann, H.; Epstein, A. J. Characterization of The 1:1 Charge-Transfer Reaction Between Decamethylferrocene and 2,3-Dichloro-5,6-dicyanoquinone (DDQ): Structure of The DDQH-anion. *J. Am. Chem. Soc.* **1982**, *104*, 4403–4410.
- (98) Reichardt, C. Solvatochromic Dyes as Solvent Polarity Indicators. *Chem. Rev.* **1994**, *94*, 2319–2358.
- (99) Lindoy, L. F. *The Chemistry of Macrocyclic Ligand Complexes*; Cambridge University Press: Cambridge, U.K., 1989.
- (100) Inoue, Y.; Gokel, G. W., Eds. *Cation Binding by Macrocycles: Complexation of Cationic Species by Crown Ethers*; Marcel Dekker: New York, 1990.
- (101) Vogtle, F.; Weber, E., Eds. *Host Guest Complex Chemistry, in Topics in Current Chemistry*; Springer-Verlag: Berlin, 1984, 1985; Vols. 121, 128.
- (102) Bourson, J.; Pouget, J.; Valeur, B. Ion-Responsive Fluorescent Compounds. 4. Effect of Cation Binding on The Photophysical Properties of A Coumarin Linked To Monoaza- and Diaza-Crown Ethers. *J. Phys. Chem.* **1993**, *97*, 4552–4557.
- (103) Valeur, B.; Leray, I. Design Principles of Fluorescent Molecular Sensors for Cation Recognition. *Coord. Chem. Rev.* **2000**, *205*, 3–40.
- (104) Lamb, J. D.; Izatt, R. M.; Swain, C. S.; Christensen, J. J. A Systematic Study of The Effect of Macrocyclic Ring Size And Donor Atom Type On The Log K, ΔH , and T ΔS of Reactions At 25 °C in Methanol of Mono- and Divalent Cations With Crown Ethers. *J. Am. Chem. Soc.* **1980**, *102*, 475–479.
- (105) Takeda, Y.; Yano, H. A Conductance Study of The Complexation Reaction of Dibenzo-24-crown-8 with Alkali Metal Ions in Propylene Carbonate and Methanol. *Bull. Chem. Soc. Jpn.* **1980**, *53*, 1720–1722.